PNNL-13748

Pacific Northwest National Laboratory
Operated by Battelle for the U.S. Department of Energy

Final Report

Mechanics of Bubbles in Sludges and Slurries

P. A. Gauglitz
G. Terrones
Pacific Northwest National Laboratory

S. J. Muller
M. M. Denn
Chemical Engineering Department
University of California at Berkeley

W. R. Rossen
Petroleum and Geosystems Engineering Department
University of Texas at Austin

Project Number – 60451
Project Duration: FY97-FY02

Prepared for the U.S. Department of Energy
under Contract DE-AC06-76RL01830

DISCLAIMER

PACIFIC NORTHWEST NATIONAL LABORATORY
operated by
BATTELLE
for the
UNITED STATES DEPARTMENT OF ENERGY
under Contract DE-ACO6-76RLO183O

Printed in the United States of America

Available to DOE and DOE contractors from the
Office of Scientific and Technical Information,
P.O. Box 62, Oak Ridge, TN 37831-0062;
ph: (865) 576-8401
fax: (865) 576-5728
email: reports@adonis.osti.gov

Available to the public from the National Technical Information Service,
U.S. Department of Commerce, 5285 Port Royal Rd., Springfield, VA 22161
ph: (800) 553-6847
fax: (703) 605-6900
email: orders@ntis.fedworld.gov
online ordering: http://www.ntis.gov/ordering.htm


This document was printed on recycled paper.
(8/00)

PNNL-13748

Mechanics of Bubbles in Sludges and Slurries

Phillip A. Gauglitz
Guillermo Terrones
Pacific Northwest National Laboratory
Richland, WA 99352

Susan J. Muller
Morton M. Denn
Chemical Engineering Department
University of California at Berkeley
Berkeley, CA 94720

William R. Rossen
Petroleum and Geosystems Engineering Department
University of Texas at Austin
Austin, TX 78712

Project Number – 60451
Project Duration: FY97–FY02

Prepared for the U.S. Department of Energy
under Contract DE-AC06-76RL01830

Pacific Northwest National Laboratory
Richland, Washington 99352

Table of Contents

Executive Summary 1

1.0 Research Objectives 5

2.0 Methods and Results 7

2.1 Summary of Experimental Studies 7

2.2 Summaries of Theoretical Studies 13

2.2.1 Solid Mechanics Studies 13

2.2.2 Fluid Mechanics Studies 17

2.2.3 Porous Media with Newtonian Fluids 21

2.2.4 Porous Media with Yield-Stress Fluids 25

3.0 Relevance, Impact, and Technology Transfer 30

4.0 Project Productivity 32

5.0 Personnel Supported 32

6.0 Publications 33

7.0 Interactions 34

8.0 Transitions 35

9.0 Patents 35

10.0 Future Work 35

11.0 Literature Cited 36

Figures

1. Example of Hysteresis in Waste Level and Barometric Pressure for Hanford Tank S-106 5

2. Bubbles Expanding in Porous Media Filled with a Newtonian Fluid or a Yield-Stress Fluid, and a Bubble Displacing a Yield-Stress Fluid 6

3. Apparatus for Pressure and Bubble Volume Measurements for Single Bubbles 9

4. Measured and Extrapolated Strength for Bentonite and Kaolin Clay Simulants 9

5. Small Apparatus Results for Bubble Volume and Pressure Changes for Bubbles in Bentonite Clay Simulants 10

6. Small Apparatus Results for Bubble Volume and Pressure Changes for Bubbles in a 140–270 Mesh Sand Bed Filled with a Range of Bentonite Clay Yield-Stress Fluids 11

7. Large Apparatus Results for Bubble Volume and Pressure Changes for Bubbles in Sand Filled with a Range of Bentonite Yield-Stress Fluids 12

8. The Role of Waste Physical Properties on the Hysteresis During Expansion and Compression of a Bubble 16

9. Strain Rate Contours for Flow of a Bingham Material Past a Rigid Sphere at Bn = 14.91 19

10. Apparent Yield Surfaces for Streaming Flow Past a Rigid Sphere at Bn=340.7. 19

11. Response of a Volume of a Single Bubble Within a Porous Medium to Liquid Pressure Change at a Fixed Bubble Mass 23

12. Schematic of Initial Distribution of a Population of Bubbles 23

13. Fit of Models to Tank Data. 24

14. Predicted Dimensionless Yield Stress of Mixture of Bubbles and Sand as Function of Solids and Liquid Volume Fraction, from Kam et al. (2002) 25

15. Model of Bubble Displacing a Yield-Stress Fluid in a Capillary Tube 26

16. Effect of Yield Stress on P-V Hysteresis for a Single Value of R/L and a Simple Distribution of R/L with Mass Transfer being Negligible 29

17. Comparison of Model Results with and without Mass Transfer on V-P Hysteresis 30

18. Comparison Between Model and Experimental Results for the Effect of Increasing Yield Stress on P-V Hysteresis for Bubbles in Porous Media 31

Executive Summary

The Hanford Site has 177 underground waste storage tanks that are known to retain and release bubbles composed of flammable gases. Characterizing and understanding the behavior of these bubbles is important for the safety issues associated with the flammable gases for both ongoing waste storage and future waste-retrieval operations. The retained bubbles are known to respond to small barometric pressure changes, though in a complex manner with unusual hysteresis occurring in some tanks in the relationship between bubble volume and pressure, or V-P hysteresis. With careful analysis, information on the volume of retained gas and the interactions of the waste and the bubbles can be determined.

The overall objective of this study is to create a better understanding of the mechanics of bubbles retained in high-level waste sludges and slurries. Significant advancements have been made in all the major areas of basic theoretical and experimental method development. In addition, the relevance of these basic developments to Hanford waste has resulted in an entirely new understanding of bubble mechanics and waste microstructure in Hanford waste tanks. This effort included both experimental and theoretical studies. Experimental developments have provided measurements of V-P hysteresis on a range of simulants. The theoretical approaches included solid-mechanics studies of bubbles in soft solids, fluid-mechanics studies of bubbles in yield stress fluids, and porous-media studies of bubbles in model porous media filled with Newtonian fluids or filled with yield-stress fuids.

For application to Hanford tanks, the most significant conclusion is that a new waste microstructure and bubble configuration must be postulated to explain the observed V-P hysteresis. This waste microstructure will impact future Hanford operations, such as salt-well pumping and salt-dissolution retrieval. Previous work had postulated either bubbles held in a continuum waste that behaved as a soft solid or bubbles trapped within the pore spaces of settled beds of salt crystals. While hysteresis with both of these microstructures has been predicted theoretically and observed experimentally, the parameter

ranges with significant hysteresis do not match well with typical Hanford waste properties. Our studies, however, also discovered a new microstructure directly linked with strong V-P hysteresis. The only reasonable microstructure to account for hysteresis is when the bubbles are trapped in the pore spaces of a settled bed of salt crystals, and the pore space itself is filled with a yield-stress fluid. This is a fundamentally new microscopic waste and bubble configuration.

In the experimental studies, results were obtained for a range of waste simulants covering soft solids, porous media, and the first-ever experiments of bubbles in porous media filled with yield-stress fluids. For experiments with porous media embedded with soft solids, substantial V-P hysteresis was measured for exceedingly weak materials. From a relevance viewpoint, the striking result for this microstructure is perhaps the most significant new understanding for the Hanford waste tanks. In conventional simulants, P-V hysteresis increases with strength. In conventional soft-solid simulants of bentonite clay, hysteresis was only apparent when the soft solid had strengths of at least a few hundred Pa. In contrast, when a soft solid was imbedded in a porous media, hysteresis was apparent for strengths below 1 Pa, or about three orders of magnitude weaker materials than in traditional simulants. This behavior was confirmed in a wide variety of simulants, and nearly identical behavior was observed over a thousand-fold range of sample volume. Other experiments investigated the roles of waste strength, the size- and time-scale of pressure fluctuations, and the grain size of porous media.

For theoretical studies of porous media embedded with yield-stress fluids, preliminary models were developed and compared with the experimental results. The observation of V-P hysteresis with this unique microstructure was unexpected and not discovered until late in the study. In seeking to validate this surprising experimental finding, a brief modeling effort was undertaken to combine the key elements of porous media, yield-stress fluids, and mass transfer. The model results compare favorably with the experimental findings. The key to the unique behavior is that the significant length scale for the displaced yield-stress fluids is much smaller in porous media than in a yield-stress fluid of infinite extent. For a

bubble displacing a yield-stress fluid embedded in a porous media, the critical-length scale is roughly the size of the pore throats. For a bubble displacing a yield-stress fluid as infinite media, the significant length scale is the bubble diameter. These two length scales differ by two or three orders of magnitude, and this is part of the underlying reason why an exceedingly weak yield-stress fluid can affect bubble mechanics if it is embedded within a fine-particle porous medium.

For the theoretical studies of porous media with Newtonian fluids, models were developed to determine the effective compressibility of bubbles in a rigid porous medium. While this model could predict V-P hysteresis and match actual tank behavior, the parameter values needed were not entirely consistent with typical waste properties. These models account for capillary forces that restrain how bubble response to pressure changes and therefore affect the compressibility of the bubbles. The model also considers the diffusive growth process in the context of strong capillary forces that may bias the distribution of bubble sizes in population and thereby alter the effective compressibility. Models were also developed for the yield stress and effective compressibility of a dispersion of gas, solids, and liquid (assumed here to be deformable), focusing on capillary interactions between solid and bubbles, and effects of these interactions on mechanical properties.

For the theoretical studies of fluid mechanics, new computational models were developed to better model the difficult problem of defining the boundary between the yielded (acts like a fluid) and unyielded (acts like solid) regions surrounding a bubble moving in a yield-stress fluid. Further modeling results were obtained to predict enhanced bubble rise as a bubble expands or contracts under the influence of gravity and changing barometric pressure. Here, the yield stress of the surrounding fluid is eventually overcome, its structure collapses, and the bubble rises within the yielded region. This problem relates directly to the Hanford issue of determining how bubbles migrate slowly in the Hanford tanks. The modeling results showed enhanced bubble-rise rates, but the magnitude of the increase was relatively small for the assumed fluid properties and pressure changes considered pertinent for Hanford.

For the solid mechanics theoretical development, the residual stresses associated with bubble expansion and contraction were rigorously included for the first time. This inclusion made an order of magnitude difference in the result when compared to previous heuristic theories. The theory considered the effects of external pressure fluctuations on the deformation history of bubbles imbedded in an elastic-plastic soft solid. For periodic pressure fluctuations, closed-form solutions were obtained in the case of a single bubble in media of infinite and finite extent. In these analyses, the amplitude of the pressure variation was considered to be sufficiently high that the von Mises yield criterion was satisfied in a finite region in the vicinity of the bubble boundary. It was assumed that within the medium, there was no stress relaxation following plastic deformation. Therefore, residual stresses were taken into account for every external compression and decompression excursion. Results show the occurrence of hysteresis of the bubble volume as a function of pressure fluctuations.

1.0 Research Objectives

Previous studies have established that 1) the waste level of Hanford tanks responds to barometric pressure changes, 2) the compressibility of retained bubbles accounts for the level changes, and 3) the volume of retained gas can be determined from the measured waste level and barometric pressure changes. However, interactions between the gas bubbles and rheologically complex waste cause inaccurate retained gas estimates and are not well understood. Figure 1 shows an example of waste level, and hence bubble volume, changing in a complex manner with changes in barometric pressure (Whitney et al. 1996). If simple ideal gas behavior occurred, the level and pressure data would fall on a single line rather than the hysteresis loop, demonstrating the dependence of bubble volume (waste level) on pressure history.

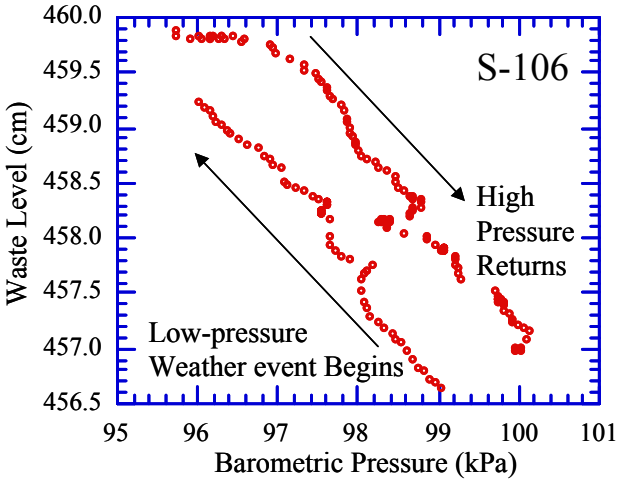

Figure 1. Example of Hysteresis in Waste Level and Barometric Pressure for Hanford Tank S-106

The objective of this research project is to gain a fundamental understanding of the interactions between gas bubbles and waste materials with representative microstructure during small pressure fluctuations. This fundamental understanding provides the mechanistic explanation for how barometric pressures changes give rise to a hysteresis between level and pressure in the Hanford tanks, which we call bubble volume and pressure, or V-P, hysteresis. This fundamental understanding will also provide a mechanistic explanation to quantify how barometric pressure fluctuations can induce the slow upward migration and release of gas bubbles in Hanford tanks.

A series of studies was conducted to develop a fundamental understanding of bubble mechanics in waste materials, including solid-mechanics modeling of bubbles in elastic-plastic soft solids, fluid-mechanics modeling of bubbles in yield-stress fluids, and porous-media modeling of bubbles in model porous media filled with Newtonian fluids or filled with yield-stress fluids. Experimental developments were also conducted to measure V-P hysteresis on a range of simulants to compare with the modeling studies. Figure 2 depicts the microstructure of bubbles in simulant systems that are the focus of these experimental and theoretical studies. At the beginning of this study, only two of these microstructures were investigated: bubbles displacing interstitial Newtonian fluid in a porous medium and bubbles displacing yield-stress fluids. Based on the experimental findings, the project objectives were expanded

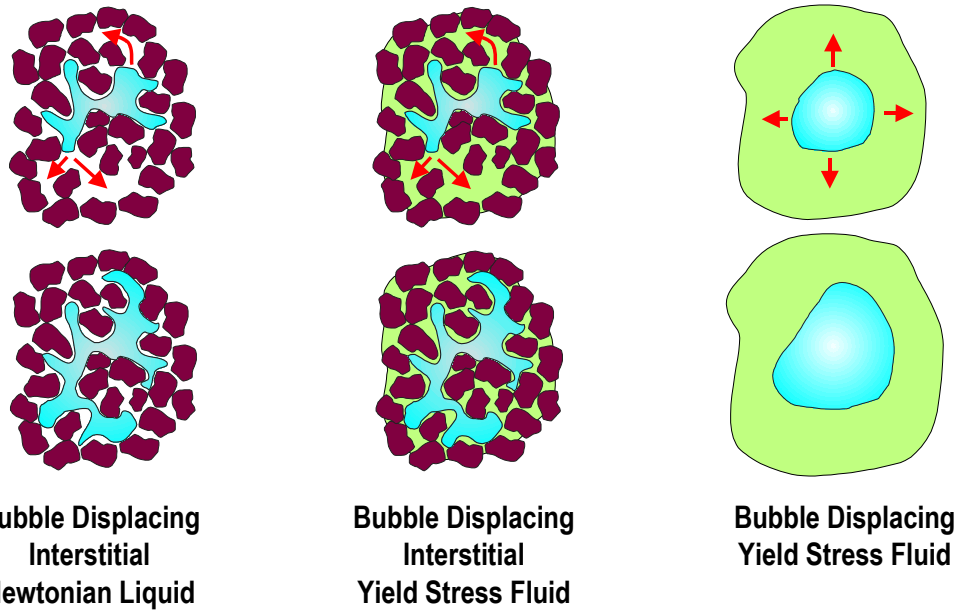

Figure 2. Bubbles Expanding in Porous Media Filled with a Newtonian Fluid or a Yield-Stress Fluid, and a Bubble Displacing a Yield-Stress Fluid

to consider bubbles displacing yield-stress fluids embedded within rigid porous media because this new microstructure was discovered to play a dominant role in V-P hysteresis. The specific research objectives for the various studies are described below.

The objective for the experimental studies was to develop techniques to quantify bubble/waste interactions by measuring small changes in bubble volume with pressure variations for a range of waste simulants. The pressure changes, and thus volume changes, are only a few percent for typical barometric fluctuations, so the measurements must be both precise and accurate. Because the waste simulants will interact with both the apparatus walls and the bubbles, the experimental results must be shown to be independent of the apparatus. Experiments with different sample volumes are conducted to confirm that measured V-P hysteresis is primarily a bubble/simulant interaction. Accordingly, a key objective with the experimental method development was collecting results at various size scales.

The objective for the solid mechanics theoretical studies was to model the effect of small pressure changes on bubble volumes. The general approach is to determine the stress-and-strain fields produced by pressure variations on a single bubble embedded in an elastic-plastic medium. The first scientific challenge is to create a fundamental approach for including residual stresses in a rigorous manner for simple pressure changes. We will then turn to the problem of periodic pressure changes, and in particular sinusoidal pressure changes. This choice retains the critical issue of retaining information on residual stresses when the pressure variation switches direction (increasing or decreasing). While natural weather events are more complicated pressure variations, the fundamental nature of repeated switches in the direction of pressure change will be addressed with the periodic changes.

The objective for the fluid mechanics theoretical studies was to address the basic scientific issue of the way in which yielding and flow occur around an expanding bubble in a yield-stress fluid. The first aspect of this study was on the outstanding issue of the existence of yielded regions in squeeze flow since

this is the most elementary prototype of a flow with compression and expansion. In particular, numerical methods were used to examine the effect of finite-length scales on the development of unyielded regions following the initiation of flow. The second aspect of the study was on the more relevant problem of flow around a sphere and expansion and contraction flow about a spherical bubble under the influence of gravity and changing barometric pressure. A key application of these studies will be a mechanistic understanding of slow bubble rise in wastes, which is a central problem in managing flammable-gas safety hazards.

The first objective for the porous media theoretical studies with Newtonian fluids was to develop models to determine the effective compressibility of bubbles in a rigid porous medium. The model must account for capillary forces that restrain how bubble response to pressure changes and therefore affects the compressibility of the bubbles. The model must also consider the diffusive growth process in the context of strong capillary forces that may bias distribution of bubble sizes in population and thereby alter the effective compressibility. The second objective was to develop models for the yield stress and effective compressibility of a dispersion of gas, solids, and liquid (assumed here to be deformable), focusing on capillary interactions between solid and bubbles, and the effects of these interactions on mechanical properties.

The objective of the theoretical studies of porous media with yield-stress fluids was to develop a model that captures the important behavior of bubbles in this microstructure. In particular, a physical model was sought to explain the capability of very weak yield-stress fluids within porous media to create significant V-P hysteresis.

2.0 Methods and Results

In the following sections, summaries are provided for the primary area of experimental results as well as theoretical studies of solid mechanics, fluid mechanics, porous media with Newtonian fluids, and porous media with yield-stress fluids.

2.1 Summary of Experimental Studies

To increase our understanding of the interactions between gas bubbles and waste materials during small pressure fluctuations, experimental techniques were developed to quantify bubble/waste interactions in a range of waste simulants. These experiments focused on measuring the relationship between bubble volume and pressure for periodic pressure variations, with a particular emphasis on quantifying the V-P hysteresis caused due to bubble/simulant interactions.

In the experimental studies, results were obtained for a range of waste simulants covering bubbles in yield stress fluids, porous media filled with Newtonian fluids, and the first-ever experiments of bubbles in porous media filled with yield-stress fluids. Striking results were found for this microstructure, and this is perhaps the most significant new understanding for the Hanford waste tanks.

Figure 3 shows the experimental apparatus used to measure small changes in bubble volume with pressure variations for a range of waste simulants. The pressure changes, and thus volume changes, are only a few percent for typical barometric fluctuations, so the apparatus was designed to give very precise

and accurate measurements. The apparatus consists of a computer-controlled pressure system that applies any pressure change, typically periodic, to the top of a test vessel. For the results reported here, a 10 min duration was set for each sinusoidal pressure cycle. Typically, three to ten cycles were needed to obtain volume and pressure data that had identical behavior with previous cycles (steady-state periodic behavior). Two different sample chambers were used—a smaller 2-cm-diameter vessel and a larger 20-cm-diameter vessel. In the 2-cm vessel, either small plugs containing a number of bubbles or individual bubbles were studied. Each vessel employed a different technique for measuring small volume changes. For the small vessel, a glass capillary was employed to magnify the minute volume changes of the bubbles into measurable level changes in the capillary. A video camera was used to record level changes in the capillary tube, and the position of the meniscus in the capillary was determined by image analysis to obtain the level as a function of pressure and time. For the large test vessel, an ENRAF level gauge was used to measure the level, again in a narrow diameter tube that amplifies the level change. System controls and image analysis are performed with National Instruments hardware and LabView software.

The level-change measurements provided data on changes in bubble volume, but not the bubble volume directly. To determine the initial volume of gas in an experiment, measurements were made of the total volume in the apparatus and the mass of each component. With known density values for water, clay, and sand, the volume occupied by gas bubbles could be determined. In the presentation of experimental results below, the data are reported as dimensionless volume as a function of a scaled pressure. For an ideal isothermal gas, the exact relationship between volume and pressure is the following:

$$\frac{V_o + \Delta V}{V_o} = \frac{P_o}{P} \tag{1}$$

where V_o and P_o are the initial volume and pressure, with P_o taken as the midpoint in the pressure cycle, and ΔV is the measured volume change when the pressure changes to P.

A variety of particulate-liquid systems have been employed. Mixtures of water and bentonite or kaolin clay were used as the yield-stress fluid. Figure 4 shows the range of shear strength measured for the clay/water systems, including values reported by Gauglitz et al. (1996) and Powell et al. (1995). Porous media systems were composed of sand (Lane Mountain Co.) that was sieved into fractions for the small vessel experiments or used without sieving in the large experiments. Within each simulant, gas bubbles were created by mixing a small volume of hydrogen peroxide with the clay and water that then decomposed over a few hours to form uniformly dispersed oxygen bubbles.

Figure 5 shows the relationship between bubble volume and pressure for bubbles in yield-stress fluids spanning a range of strengths. The plots also show the behavior of an ideal gas for comparison. For weaker simulants at lower clay content, the measured bubble volume and pressure has essentially the same behavior as an ideal gas. That is, the gas bubbles expand and compress as an ideal gas and are not influenced by the presence of this surrounding soft solid. For stronger materials at higher clay content, the change in bubble volume with pressure shifts from the ideal gas behavior. A significant observation is that the spread in the V-P hysteresis loop remains narrow while the slope of the loop becomes shallower. This shape contrasts with the behavior for Tank S-106 shown above in Figure 1. These bentonite experiments are for strengths ranging from approximately 100 to 15,000 Pa. Even at the very highest in

strengths, the width of the V-P hysteresis was less dramatic than what was measured in the actual Hanford tanks. The onset of V-P hysteresis begins at 27-wt% bentonite, which is about 3000 Pa.

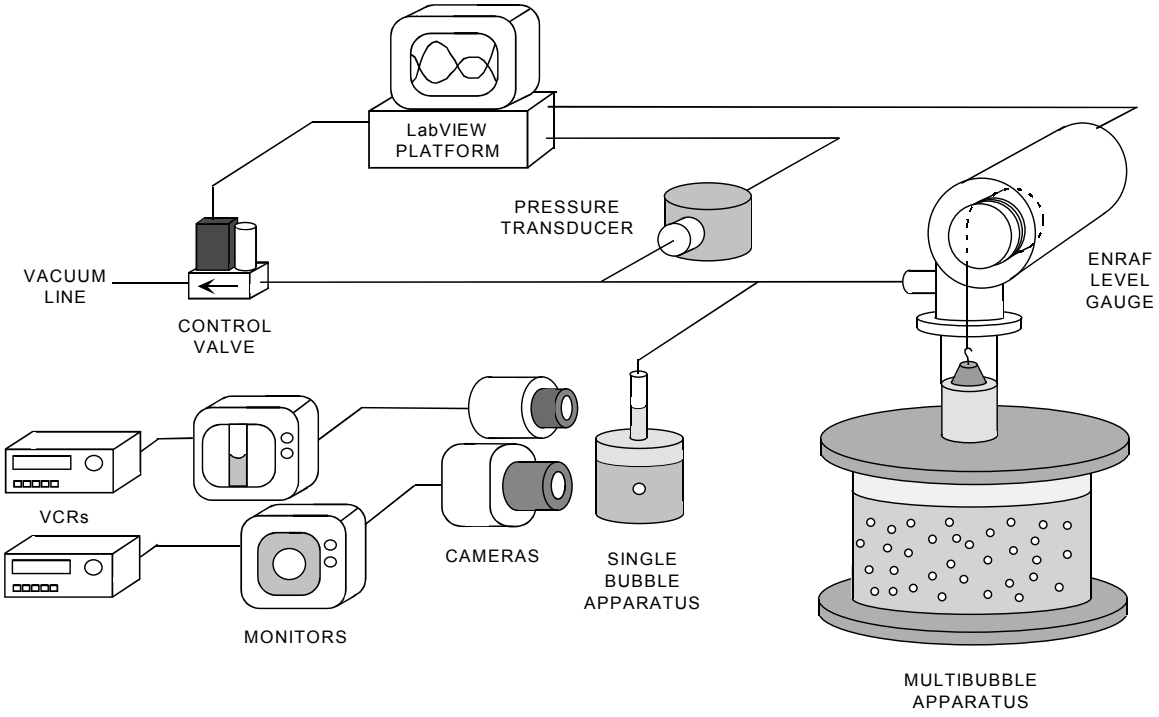

Figure 3. Apparatus for Pressure and Bubble Volume Measurements for Single Bubbles

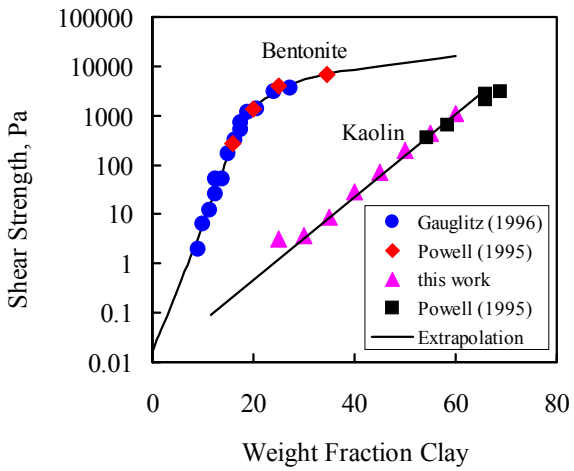

Figure 4. Measured and Extrapolated Strength for Bentonite and Kaolin Clay Simulants

Figure 6 shows the behavior of bubbles in porous media that are imbedded with very weak yield-stress fluids. The apparatus was essentially the same as that used for the bentonite simulants. Figure 6 also shows the ideal gas behavior for comparison. The results show that for sufficiently weak materials, or low clay content, the bubble behavior is equivalent to an ideal gas. That is, the bubbles expand and

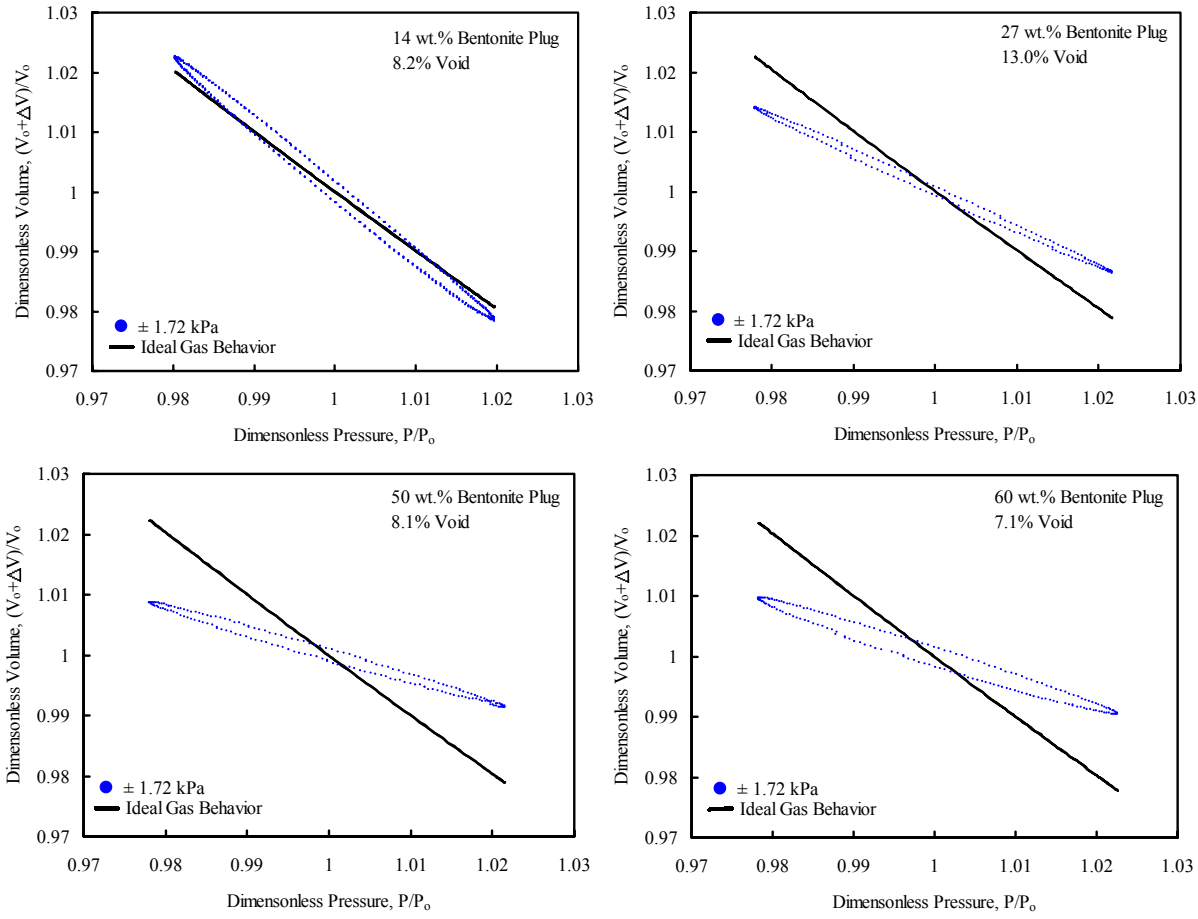

Figure 5. Small Apparatus Results for Bubble Volume and Pressure Changes for Bubbles in Bentonite Clay Simulants

contract within the pore space of the porous media and are not affected by the presence of the weak yield-stress fluid being displaced inside the pore space. It is also important to note that capillary forces are not causing measurable V-P hysteresis. As the strength and clay content of the pore fluid increases, the bubble volume pressure relationship shows progressively more hysteresis. There are two distinct observations. First, the V-P hysteresis loop becomes broader but generally follows the slope of the ideal gas behavior. With stronger yield-stress fluids within the pores, or higher clay content, the V-P hysteresis loop becomes more horizontal. Eventually, at the highest clay content of 10 wt%, the V-P hysteresis loop shows relatively small changes in bubble volume with pressure.

Figure 6 shows the behavior of bubbles in porous media that are imbedded with very weak yield-stress fluids. The apparatus was essentially the same as that used for the bentonite simulants. Figure 6 also shows the ideal gas behavior for comparison. The results show that for sufficiently weak materials, or low clay content, the bubble behavior is equivalent to an ideal gas. That is, the bubbles expand and contract within the pore space of the porous media and are not affected by the presence of the weak yield-stress fluid being displaced inside the pore space. It is also important to note that capillary forces are not causing measurable V-P hysteresis. As the strength and clay content of the pore fluid increases, the bubble volume pressure relationship shows progressively more hysteresis. There are two distinct

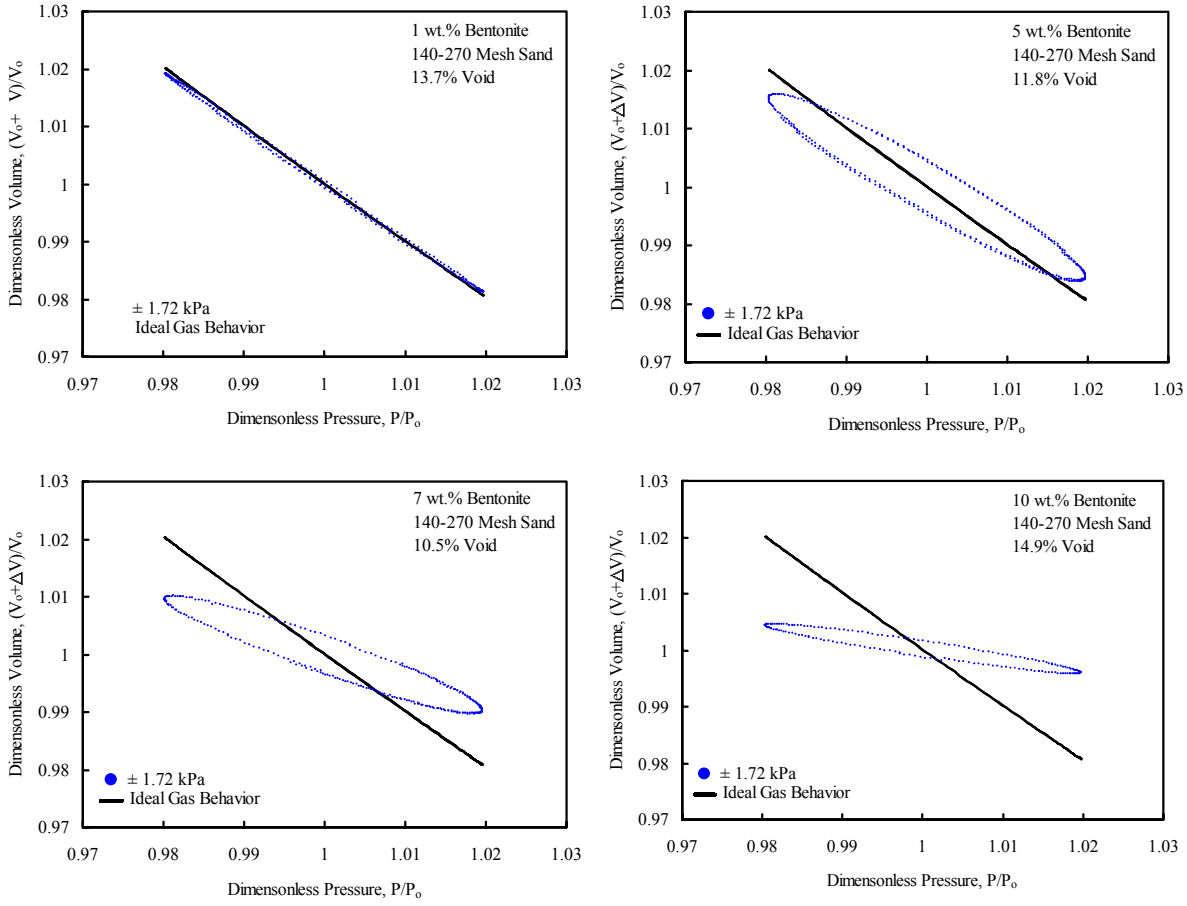

Figure 6. Small Apparatus Results for Bubble Volume and Pressure Changes for Bubbles in a 140–270 Mesh Sand Bed Filled with a Range of Bentonite Clay Yield-Stress Fluids

observations. First, the V-P hysteresis loop becomes broader but generally follows the slope of the ideal gas behavior. With stronger yield-stress fluids within the pores, or higher clay content, the V-P hysteresis loop becomes more horizontal. Eventually, at the highest clay content of 10 wt%, the V-P hysteresis loop shows relatively small changes in bubble volume with pressure. For these experiments, the onset of V-P hysteresis occurs at about 5-wt% bentonite. Extrapolation of the shear-strength date in Figure 4 gives an estimate of a few tenths of a Pa. In comparison to Figure 5 where deviations from ideal gas began at about 3000 Pa, in porous media, V-P hysteresis occurs with yield-stress materials having about three to four orders of magnitude lower strength.

Additional experiments were conducted with a different yield-stress fluid, kaolin clay mixtures, to confirm this observation that very weak yield-stress fluids within porous media give rise to significant V-P hysteresis. These experiments showed the onset of V-P hysteresis between 10 and 20-wt% kaolin. The estimated strength in Figure 4 for this range of kaolin is a few tenths of a Pa, which is the same strength range for the onset of V-P hysteresis in bentonite yield-stress fluids. Further experiments were attempted with carbopol gels, but the addition of hydrogen peroxide to generate bubbles also degraded the carbopol, making this simulant unusable.

Further experiments were conducted in the small apparatus to investigate the role of the pore size. The characteristic scaling for yield-stress fluids in porous media is described by Eq. 20 in a theoretical section below. For larger pores, the V-P hysteresis should be smaller and the V-P hysteresis should increase with decreasing pore size. For these experiments, tests used a bentonite fluid with 5-wt% clay in four mesh ranges of sand (40–70, 70–140, 140–270, and 270–400). For the coarsest fraction of 40–70 mesh, the V-P hysteresis was negligible, and the V-P hysteresis became progressively larger for the finer mesh fractions. These results further support the fundamental physical mechanism of bubbles displacing the yield-stress fluids within the pores and the dominant mechanism leading to V-P hysteresis.

Larger scale experiments were conducted to further quantify the V-P hysetersis observed for porous media filled with yield-stress fluids. Figure 7 shows the results for bubble volume and pressure for the range of bentonite fluids studied in the small apparatus. The larger test vessel had a sample volume 1000 times larger than the small test vessel. The results show a very similar onset of V-P hysteresis, with substantial deviations from ideal gas behavior at about 3-wt% bentonite. Again, the extrapolation indicates that the strength is below 1 Pa. With essentially identical results for V-P hysteresis over a thousand-fold range of sample volume, this confirms the conclusion that the V-P hysteresis is dominated by the behavior of yield-stress fluids in porous media.

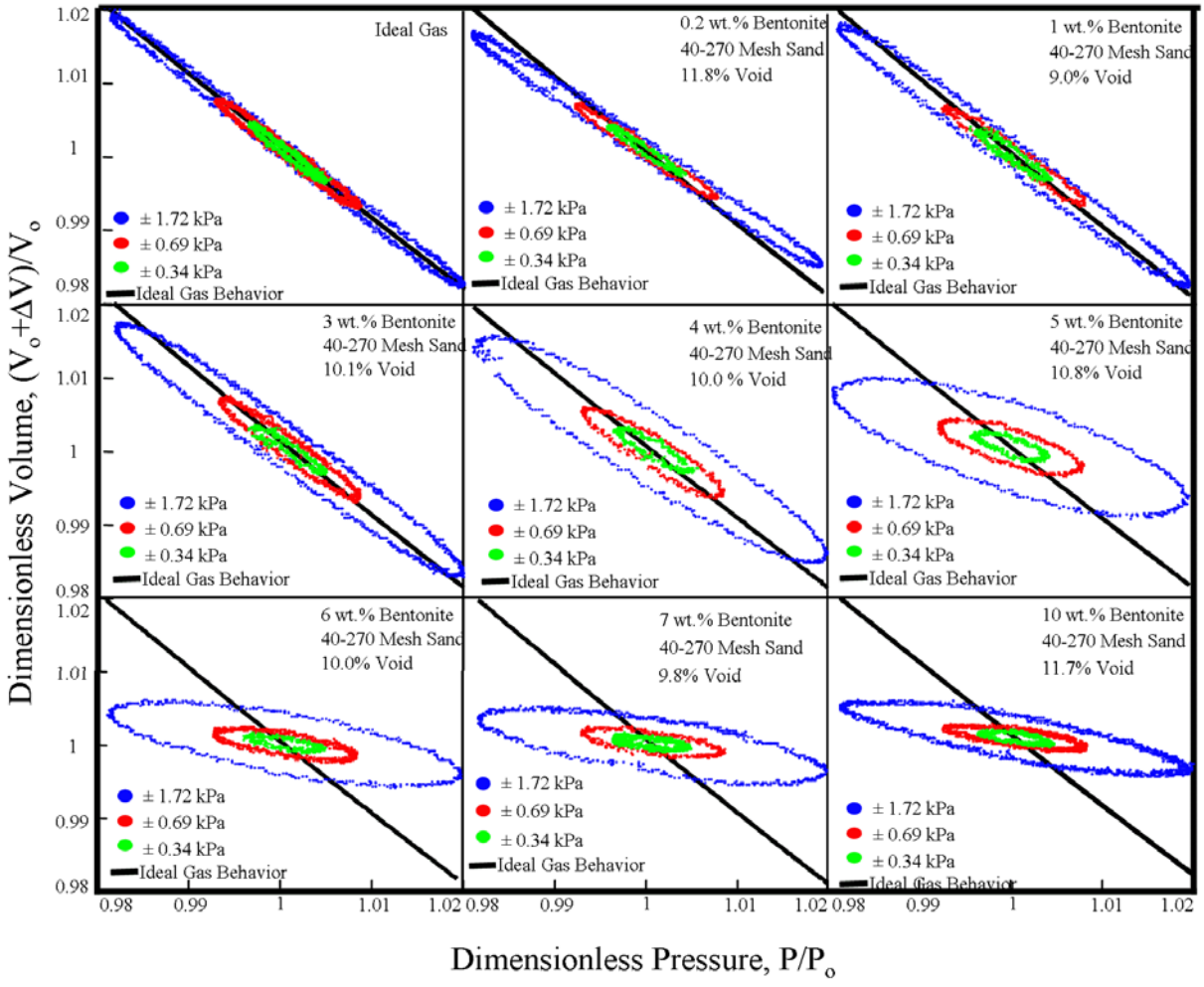

Figure 7. Large Apparatus Results for Bubble Volume and Pressure Changes for Bubbles in Sand Filled with a Range of Bentonite Yield-Stress Fluids

In addition to the key observation that exceedingly week yield-stress fluids within porous media create significant V-P hysteresis, there are additional significant observations revealed in Figure 7. First, as the yield-stress fluid increases strength, the V-P hysteresis loop both becomes wider and then the slope becomes shallower. For the yield-stress fluid in Figure 5, the V-P hysteresis loop became shallower, but never became wide. The actual tank data shown in Figure 1 have a relatively wide hysteresis loop. Second, the experimental results at the ends of the loops (highest and lowest pressures) show the bubble volume continuing to increase (or decrease) even after the pressure change has reversed direction. That is, once the pressure reaches a minimum and begins increasing, the bubbles still continue to expand. This behavior is not readily explained by the behavior of a yield-stress fluid. Transient processes, such as mass transfer, provide a possible explanation. Because of this character in the experimental data, a model combining mass transfer with a yield-stress fluid in porous media was developed and will be discussed in Section 2.2.4.

2.2 Summaries of Theoretical Studies

Theoretical as well as experimental studies are needed in the effort to understand gas bubbles in waste materials. Theoretical studies that were undertaken included solid mechanics, fluid mechanics, and porous media.

2.2.1 Solid Mechanics Studies

The compression and expansion of bubbles in elastic-plastic soft solids were studied to model the effect of small pressure changes on bubble volumes and predict V-P hysteresis. In comparison to previous mathematical studies (Whitney et al. 1996), this work rigorously includes residual stresses when the pressure switches from decreasing to increasing, and the reverse, and it includes a more rigorous yield criterion and coupling of elastic and plastic regions of deformation. While this study considers a time-dependent problem, the approach assumes a quasi-steady state where transient stresses are neglected, and time is simply a parameter. Inherently transient problems, such as bubble rise, are addressed is the following section on fluid mechanics. In this section, the theoretical analysis of the deformation of a single bubble in a compressible elastoplastic isotropic medium under external pressure fluctuations is briefly described. A general situation is considered in which the external pressure fluctuations are large enough to produce plastic zones during compression and reversed plastic zones during decompression. It is assumed that the rate of change of the pressure variations acting on the medium is sufficiently small that the inertial or dynamic effects become negligible. Under the condition of radial quasi-static expansion and contraction of the bubble, the equilibrium and compatibility equations are used to determine the state of elastic stress and strain within the medium. To determine the plastic stresses, the equations of equilibrium and the yield criterion must be satisfied. Yield is assumed to occur in the continuum according to the von Mises criterion.

Because of the symmetry of the problem, the only non-vanishing component of the displacement vector is in the radial direction. In addition, the state of stress in the angular directions is isotropic. Furthermore, the directions of the principal stresses correspond to those of the coordinate system. This implies that the radial and angular strains in the plastic regions can be represented by their corresponding logarithmic strains because the principal stresses coincide with the coordinate axis (Lubliner 1990).

With the above assumptions and the simplifications due to spherical symmetry, the governing equations for the stresses and strains in the elastic region are

$$\begin{bmatrix} \nu & \nu-1 \\ 1 & 0 \end{bmatrix} \frac{d}{dr} \begin{Bmatrix} \sigma_r \\ \sigma_\theta \end{Bmatrix} + \frac{1}{r} \begin{bmatrix} \nu+1 & -\nu-1 \\ 2 & -2 \end{bmatrix} \begin{Bmatrix} \sigma_r \\ \sigma_\theta \end{Bmatrix} = 0 \tag{2}$$

$$\begin{Bmatrix} \dot{\varepsilon}_r \\ \dot{\varepsilon}_\theta \end{Bmatrix} = \frac{1}{E} \begin{bmatrix} 1 & -2\nu \\ -\nu & 1-\nu \end{bmatrix} \begin{Bmatrix} \sigma_r \\ \sigma_\theta \end{Bmatrix} \tag{3}$$

where

r	=	radial coordinate
σ_r and σ_θ $(= \sigma_\phi)$	=	radial and angular stresses
ν	=	Poisson ratio
$\dot{\varepsilon}_r$ and $\dot{\varepsilon}_\theta$	=	radial and angular strain rates
E	=	Young's modulus of elasticity.

The initial and boundary conditions for the elastic problem in a medium of infinite extent are

$$\varepsilon_r(r;0) = \varepsilon_\theta(r;0) = 0, \qquad \sigma_r(r;0) = \sigma_\theta(r;0) = -p_o \tag{4}$$

$$\sigma_r(a;t) = -p_o\left(\frac{a_o}{a}\right)^3, \qquad \sigma_r(\infty;t) = -p_o + p_A \sin\left(\frac{2\pi t}{T}\right) \tag{5}$$

where a_o is the initial bubble radius; a is the current radius, which is an unknown function of the external pressure; and the external pressure exerted on the medium is periodically varied in time t with a period T. When the outer boundary is finite, the number of equations for the elastic and plastic deformations is twice that of infinite media. At each pressure sweep, the expressions for these deformations are obtained analytically but solved numerically because they involve nonlinear implicit functions.

The conditions given in Eq. 5 correspond to realistic boundary conditions because the internal bubble pressure is implicitly coupled to the bubble radius, and the pressure fluctuations are externally applied to the medium. It was assumed that the bubbles contain an ideal gas and the compression/expansion of the bubble is isothermal. During any given pressure sweep, the continuum in general comprises a finite plastic region and an infinite elastic region. As time evolves, the alternate compression and decompression cycles create states of residual stress that constitute the initial conditions for the subsequent pressure sweep. For a given pressure sweep, two different sets of equations are solved to determine the plastic and elastic states of stress and strain. Two additional boundary conditions are introduced: the yield criterion is satisfied at the plastic-elastic boundary (which is not known a priori), and the stresses are continuous across this boundary.

When a finite plastic zone is formed, the equations for the stresses and the finite displacements are

$$\begin{bmatrix} r & 0 \\ 0 & 0 \end{bmatrix} \frac{d}{dr} \begin{Bmatrix} \sigma_r \\ \sigma_\theta \end{Bmatrix} + \begin{bmatrix} 2 & -2 \\ (-1)^n & (-1)^{n+1} \end{bmatrix} \begin{Bmatrix} \sigma_r \\ \sigma_\theta \end{Bmatrix} = \begin{Bmatrix} 0 \\ \sigma_y \end{Bmatrix} \tag{6}$$

$$\ln\left(\frac{r^2\, dr}{r_o^2\, dr_o}\right) = \frac{1-2\nu}{E}(\sigma_r + 2\sigma_\theta) + \left[\varepsilon_r + 2\varepsilon_\theta - \frac{1-2\nu}{E}(\sigma_r + 2\sigma_\theta)\right]\Bigg|_{t=\text{Onset of Yield}} \tag{7}$$

$$\varepsilon_r = \ln\left(\frac{dr}{dr_o}\right), \qquad \varepsilon_\theta = \ln\left(\frac{r}{r_o}\right) \tag{8}$$

where

n	=	0 or 1 during external compression or decompression, respectively
r	=	current radial coordinate
r_o	=	original radial coordinate
σ_y	=	yield stress of the material in pure tension.

The initial conditions for the plastic displacements are obtained from the state of stress-strain at the onset of yield. This is calculated by evaluating the elastic solution at the critical pressure (above which there is plastic yield). For the combined plastic and elastic problems, the boundary conditions are

$$\sigma_r^p(a) = -p\left(\frac{a_o}{a}\right)^3, \qquad \sigma_r^e(b) - \sigma_\theta^e(b) = (-1)^n \sigma_y \tag{9}$$

$$\sigma_r^p(b) = \sigma_r^e(b) \qquad \sigma_\theta^p(b) = \sigma_\theta^e(b) \tag{10}$$

$$\sigma_r^e(\infty) = -p_o + p_A \sin\left(\frac{2\pi t}{T}\right) \tag{11}$$

where the superscripts p and e denote plastic and elastic solutions, respectively. After reaching the maximum decompression, the external pressure is increased, and compression begins by retracing the same pressure values followed by the previous sweep. However, at the same pressure value, the state of stress during compression is different from that of decompression because of the presence of residual stresses. Residual stresses are the sum of the original state of stress (before the beginning of compression) and the elastic stresses originating from the departure of the state of stress from the maximum decompression point (Chadwick 1959; Hopkins 1960). Initially, compression causes a state of elastic stress that is followed by the formation of a reversed plastic zone. During this pressure sweep, the elastic and plastic equations are solved by taking into account that the extent of the new plastic zone is different from that obtained during decompression and that the bubble radius has changed because of an irrecoverable plastic displacement. For a detailed account of this procedure and its generalization to an arbitrary number of pressure sweeps, refer to Terrones and Gauglitz (in preparation).

Figures 8a and 8b show example predictions for the changes in the bubble radius as the pressure is periodically varied. Starting at the highest pressure point on any V-P hysteresis loop, decompression begins with a slow change in bubble radius. The rate of increase in the bubble radius markedly increases after the formation of a plastic zone and continues until the lowest pressure is reached. From the beginning of compression at this point, the medium loads elastically to a critical pressure below which the material loads plastically until the maximum compression point is reached. This behavior repeats during subsequent pressure cycles. The V-P hysteresis is shown by the bubble radius depending on pressure history even though the bubble contains an ideal gas. If the bubble were subjected to a hydrostatic compression or expansion, the dependence of bubble radius on time-periodic pressure would produce a single curve rather than a loop.

Figure 8b shows that increasing the waste strength causes a wider V-P hysteresis loop in the relationship between bubble radius and pressure. This occurs because the waste, which is a soft solid, resists the expansion and compression of the bubble. Figure 8a shows that the hysteresis depends on Young's Modulus as well. In comparison to earlier studies (Whitney et al. 1996), these theoretical results that include residual stresses and the von Mises yield criterion predict V-P hysteresis loops with widths that are about an order of magnitude wider.

The predicted behavior in Figures 8a and 8b differs from the experimental results for a yield-stress fluid shown in Figure 5. In the laboratory studies, the V-P hysteresis loop is narrow with a slope that becomes shallower with increasing strength. While the predicted V-P hysteresis shows a shape similar to the actual tank data shown in Figure 1, the laboratory results do not confirm these results. It is likely that the selected elastic-plastic model is too simple to represent the laboratory simulants, and the similarity of the predicted results with the actual tank behavior is fortuitous.

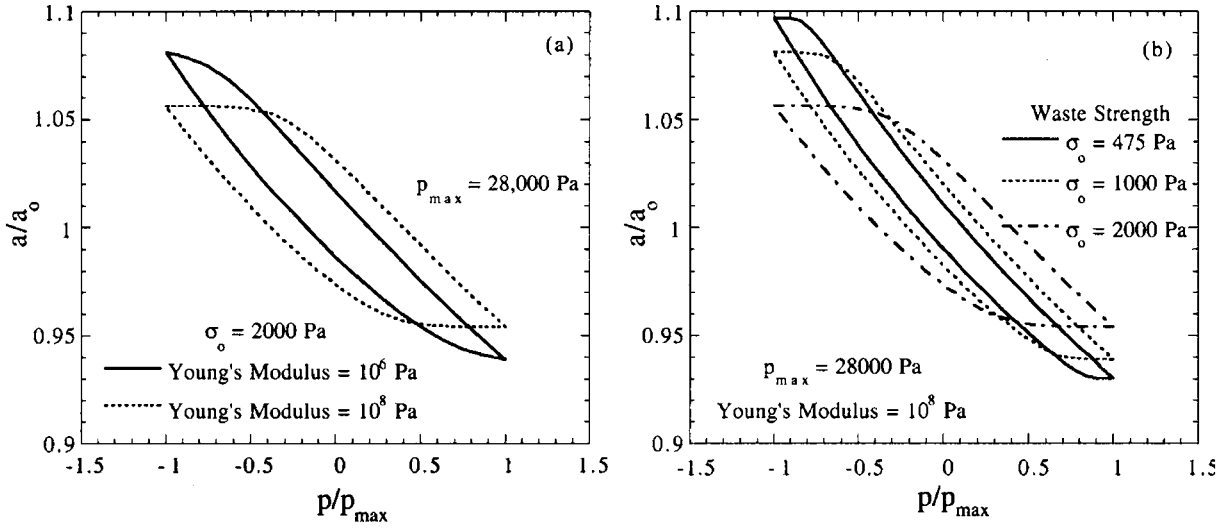

Figure 8. The Role of Waste Physical Properties on the Hysteresis During Expansion and Compression of a Bubble: a) Effect of Yield Stress, b) Effect of Modulus of Elasticity

2.2.2 Fluid Mechanics Studies

To improve our ability to address dynamic problems, such as bubble/waste interactions with motion, this study is focused on developing a better understanding of the basic scientific issue of the way in which yielding and flow occur with a yield-stress fluid in selected problems. Denn and Marrucci (1999) have reported on the initial study of yield surfaces in squeeze flow and Lui et al. (in press) present subsequent studies for spheres. A summary of the results for spheres is reported here. The fluid mechanics of bubbles in visco-plastic fluids was studied to address the way in which yielding and flow occur around an expanding bubble in a yield-stress fluid. Creeping flows (Re=0) of a yield-stress material past a rigid sphere and a bubble were studied numerically with two aims in mind: 1) to gain insight into how to locate yield surfaces and determine their interaction in complex flows of these materials and 2) to determine the effect of pressure fluctuations on the slow rise of bubbles in yield-stress materials. Both goals are directly relevant to understanding the interaction and rise of bubbles in retained in waste storage tanks.

Yield-stress materials were described by a continuous constitutive equation characterized by a regularization parameter P_B ; this approximation of the discontinuous Bingham model was used to facilitate numerical computations. The stress tensor, $\underline{\underline{\tau}}$, in this equation is related to the rate-of-strain tensor, $\underline{\underline{D}}$, the plastic viscosity, η_p, and the yield stress, τ_y, by:

$$\underline{\underline{\tau}} = \left(\eta_p + \frac{\tau_y}{\sqrt{\frac{1}{2} II_{\underline{\underline{D}}} + \frac{P_B^{-1} R}{V}}} \right) \underline{\underline{D}} \qquad (12)$$

where II_D is the second invariant of the rate of strain tensor, and R and V are characteristic length and velocity scales, respectively. As the regularization parameter P_B tends to infinity, this model approaches the Bingham model: when the local stress falls below the yield stress, the material behaves as a rigid solid; above the yield stress, the material deforms as a viscous liquid. Flows of yield-stress materials can be characterized in terms of a Bingham number, defined as $Bn = 2\tau_y R/\eta_p V$. The boundaries between *unyielded* regions that behave as rigid solids and *yielded* regions that flow are known as *yield surfaces.*

2.2.2.1 Creeping Flow Past a Rigid Sphere: Numerical Studies

We first considered the problem of a rigid sphere of radius R translating at a fixed velocity V relative to an incompressible, isothermal Bingham material of infinite extent. The flow is assumed to be axisymmetric about the axis of translation, so it is convenient to use a cylindrical (r,z) coordinate system centered on the sphere. Both velocity components vanish at the sphere surface, while the far-field velocity has a magnitude V in the z-direction. We assume creeping flow (Re=0), so the flow is fore-aft symmetric; i.e., z=0 corresponds to a plane of symmetry.

The continuity and Cauchy momentum equations for creeping flow of an isothermal, incompressible fluid are:

$$\nabla \cdot \underline{v} = 0 \tag{13}$$

$$\underline{0} = -\nabla p + \nabla \cdot \underline{\underline{\tau}} \tag{14}$$

where p is the scalar pressure, which includes the body force. These conservation equations are solved together with the constitutive equation for the velocity, stress, deformation rate, and pressure fields using the finite-element method. A large, finite domain replaced the infinite domain, and a solution was sought over the entire computational domain, including both yielded and unyielded regions. The computational domain was discretized into a mesh consisting of nine-noded Lagrangian quadrilateral elements. The velocity field was solved using a biquadratic penalty finite element method in which the pressure in the momentum equation is approximated as $p = -\lambda \nabla \cdot \underline{v}$, where λ is the penalty parameter; a value of $\lambda = 10^6$ was used in the calculations. Reduced (2x2) Gaussian quadrature was used to evaluate the finite-element integral terms involving the penalty parameter, and 4x4 quadrature was used for all other terms. The nonlinear equations were solved by successive substitution, using the Newtonian solution as a first approximation. The drag coefficient C_s and the shape of the apparent yield surface were calculated from the stress and pressure fields where the drag coefficient is defined as $C_s=F_{drag}/6\pi\eta_p VR$, and F_{drag} is the drag force on the sphere.

Sample contours of constant strain-rate are shown in Figure 9 for a Bingham number of 14.91; within a few radii of the sphere, the yield-stress material is undergoing fluid deformation; away from the sphere, the material is unyielded. This contrasts sharply with the Newtonian fluid case, where the effect of the sphere on the medium is long range and dies off away from the sphere only as 1/r.

Determination of the position of the yield surface, however, is not straightforward. The apparent yield surface, the locus of points where the stress equals the yield stress, varies with regularization parameter P_B. This is shown in Figure 10a for Bn=340.7. Two interior unyielded regions, one attached at the poles and the other detached but adjacent to the sphere along the equatorial plane, are observed for small values of P_B, but both decrease in size with increasing P_B and seem to disappear in the limit. The yielded region increases in size with increasing P_B up to a value of $P_B = 10^8$, beyond which numerical error becomes evident in the strain-rate profiles. Profiles of the second invariant of the deformation rate (II_D) along the symmetry axis and the equatorial plane demonstrate that the flow field within the yielded region converges rapidly with respect to the regularization parameter. The position of the outer yield surface can be identified from the locus of inflection points of the logarithm of the second invariant of the deformation rate II_D scaled with the second invariant of the deformation rate at the yield stress. Apparent unyielded regions attached to the sphere at the poles and near the sphere on the equatorial plane appear to shrink to a point with increasing regularization parameter. Further studies are underway to assess the general applicability of this approach to determining the yield surfaces, for example, to the case of interacting spheres and bubbles.

2.2.2.2 Bubble Rise in an Oscillating Pressure Field: Experiments and Numerical Studies

Experimental and computational studies were undertaken to investigate the effect of pressure fluctuations on the slow rise of bubbles in yield-stress materials. The expansions and contractions of bubbles as a result of pressure changes cause a decrease in the local apparent viscosity near the bubble; the resulting drag reduction may account for some of the enhanced bubble migration thought to occur in waste tanks.

Experimental studies were performed using aqueous dispersions of Carbopol (Carbopol EZ-1, BF Goodrich). These dispersions exhibit a high degree of optical clarity and negligible gas solubility. Dispersions of 0.1 to 0.2 wt% in aqueous sodium hydroxide solution were used. A Haake RV-20 viscometer with a shear vane attachment and a Rheometrics RMS-800 with a 25-mm serrated parallel plate fixture were used for rheological characterization.

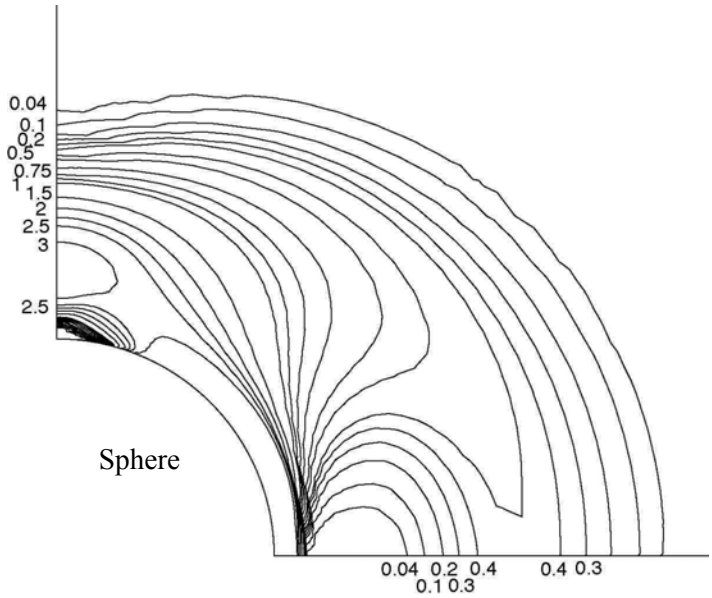

Figure 9. Strain Rate Contours for Flow of a Bingham Material Past a Rigid Sphere at Bn = 14.91

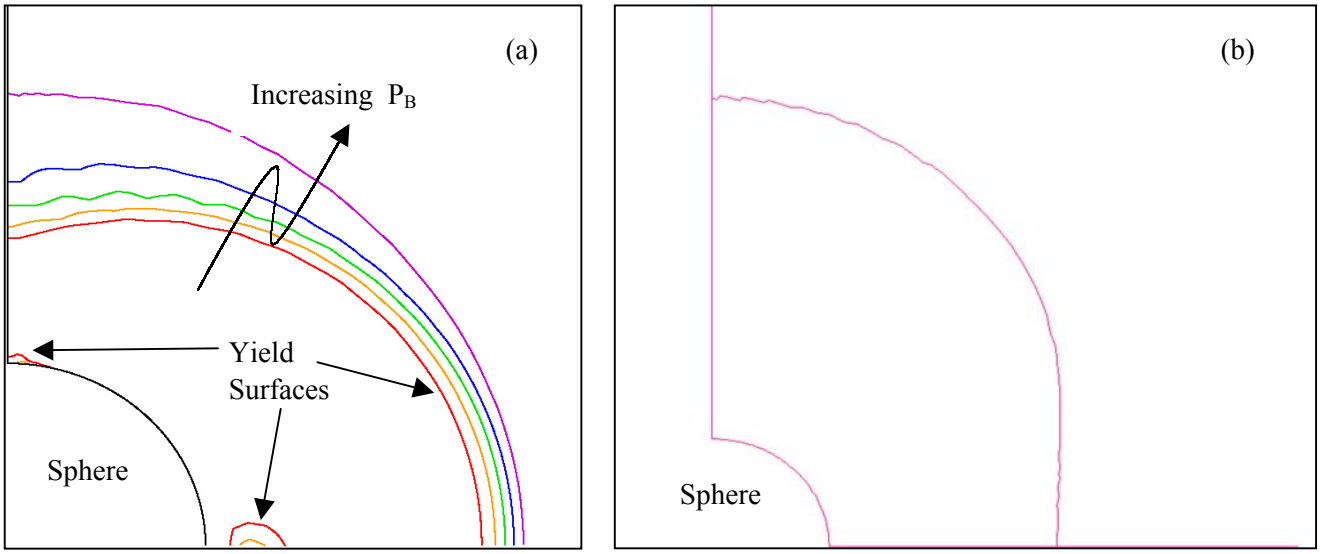

Figure 10. Apparent Yield Surfaces for Streaming Flow Past a Rigid Sphere at Bn=340.7. a) Apparent yield surfaces for varying regularization parameter. As P_B increases, the outer yield surface moves to larger r; the small, internal unyielded regions near the pole and on the equatorial plane shrink to a point. b) The limiting yield surface.

Experiments were performed in a modified graduated cylinder (5 cm in diameter and 20 cm in height). A sidearm port near the bottom of the vessel allowed for injection of gas bubbles via syringe. Injected bubbles were typically about 5 mm in diameter, resulting in a 10:1 tube-to-bubble ratio. The top of the vessel connected to the vacuum source with a ground-glass joint. All experiments were run at slightly below atmospheric pressure; pressure oscillations were controlled using a Labview (National Instruments) PID control system running on a Windows platform, and images of the bubbles were captured with a video recorder. After injection of the bubble, the system was allowed to equilibrate for at least an hour. The pressure was slowly decreased to various pressures and the rise rate (or lack thereof) was measured. Sinusoidal pressure oscillations were then imposed, and each experiment was allowed to continue for at least 10 cycles.

Numerical simulations were performed using a custom-developed finite-element fluid mechanics program. A shear-free boundary was enforced at the sphere surface, with a radial velocity corresponding to the magnitude of the bubble expansions or contractions. The dimensionless Stokes drag coefficient, C_s defined above, was calculated as a function of Bingham number, $Bn = 2\tau_y R / \eta_0 V$, and surface velocity on the sphere, V_s. The buoyant force can also be calculated from a force balance on the bubble; the buoyant force is used to calculate the yield parameter $Y_G = \tau_y / 2R\Delta\rho g$, where $\Delta\rho$ is the density difference between the bubble and the medium, and g is the acceleration due to gravity. The yield parameter can be thought of as the strength of the material relative to the gravitational force on the sphere.

For experiments with $Y_G > 0.8$, no bubble rise was seen for any value of surface velocity, V_S. The imposed pressure oscillations in some cases affected the material even after the oscillations were halted: this is believed to be caused by the thixotropy of the Carbopol dispersions. Discounting data in which this shear-history was evident, the criteria for bubble rise in the absence of pressure oscillations was found to be $Y_G \approx 0.6$; oscillating bubbles were observed to rise at values above 0.7. This rise enhancement does not, however, seem adequate to explain the enhanced rise rates in the waste tanks, which would require an order of magnitude (or greater) increase in the value of Y_G for incipient rise. The role of thixotropy in the enhanced bubble rise, both in tank waste and in Carbopol, is yet unknown and would require further characterization.

The numerical simulations indicated that in the absence of pressure oscillations (zero surface velocity), the criterion for incipient rise is $Y_G = 0.066$, which differs from the experimental values measured in this work (~0.6) by about an order of magnitude. The discrepancy between simulation and experiment is not unexpected since Carbopol deviates significantly from the Bingham model; moreover, literature values for the incipient motion of rigid spheres show an approximately fivefold variation between experimental (~0.2) and computational (~0.04 to 0.08) results (Chhabra 1993).

As the value of V_s/V is increased, this value of Y_G for incipient rise increases, indicating that the presence of radial surface motion allows a given bubble to rise at the same rate as a more buoyant bubble with a surface velocity of zero. This indicates that pressure oscillations should, indeed, provide some degree of enhanced bubble rise. The experimental results showed less enhanced rise than predicted by simulations; this may be related to the deviation of the experimental fluid from the simple Bingham plastic ideal. Both experiments and simulations indicate that little or no observable rise enhancement by the single-bubble mechanism explored here would occur in the waste tanks due to barometric pressure

fluctuations. Bubble rise due to interactions of multiple bubbles—and the interaction of the yielded regions—remains to be explored as a mechanism for bubble-rise enhancement in the waste tanks.

2.2.3 Porous Media with Newtonian Fluids

The waste slurries stored at Hanford often have a sediment bed of settled particles that can behave as a rigid porous medium with fluid and bubbles filling the pore space, particularly for waste with coarse particles. For wastes with relatively small particles, the waste behavior is better described as a continuum yield-stress fluid and modeled with the solid and fluid mechanics approaches described in the previous sections.

Bubbles in rigid porous media filled with Newtonian fluids were studied to develop models to determine the effective compressibility of bubbles in this waste microstructure as they expand and contract in response to ambient pressure changes. Determining the effective compressibility of bubbles in the slurry could allow one to make improved estimates of the quantity of gas trapped in the slurry from changes in slurry volume with ambient pressure changes. More broadly, the diffusive growth and mechanical properties of bubbles in a porous medium is an important issue in a number of applications.

Kam et al (2001a) summarize numerical calculations based on a one-dimensional biconical-pore-network model. Figure 11 shows that a bubble will have jumps in volume as the pressure is smoothly increased or decreased. These results represent the fundamental mechanism for why the effective compressibility of a population of bubbles has V-P hysteresis with pressure increase and decrease. This hysteresis is caused by the sudden jumps of interfaces from pore throat to throat during a pressure decrease and from pore body to body during a pressure increase.

It is necessary to choose an initial distribution for the bubble population before calculating the response of this distribution to a pressure fluctuation. Care is needed to avoid bias in selecting this initial distribution; as pressure changes, the many bubbles growing or shrinking continuously show very small compressibility, while the few bubbles making jumps show very large compressibility. For instance, an initial distribution consisting of bubbles just about to jump would show large compressibility, while a group not jumping would have small compressibility. Within the slurry in the sediment layer of waste tanks, bubbles slowly grow by diffusion from the surrounding liquid. A model was developed (Kam and Rossen 2000) to simulate bubble growth induced by supersaturation and the compressibility of these bubbles subjected to a sudden change in pressure in a spherical-pore network with connectivity. If capillary forces are strong, they can affect the diffusive mass flux to individual bubbles and distort the distribution of bubbles over time, altering the effective compressibility of the population of bubbles. Figure 12 shows our approach. We selected a group extending from bubbles that have just made one jump to those on the verge of the next jump. We assume that bubble mass (moles) n_{bD} is uniformly distributed between these two limits. One could reconstruct the behavior of a broad population of bubbles using a weighted average of such groups.

The next step is to fit model parameters to changes in waste level in response to barometric pressure changes in the tanks (Kam et al. 2001b). A one-dimensional biconical-pore-network model successfully fits the trend of measured data for tank S-106 shown in Figures 1 and 13. Assuming that capillarity is the cause of this hysteresis, fitting the waste-level changes in the tanks implies that bubbles in the sediment layer are long and the ratio of pore-body radius to pore-throat radius is close to 1. Unfortunately,

compressibility cannot be quantified unambiguously from the data without additional information on pore geometry. Therefore, determining the quantity of gas in the tanks requires more than just waste-level data. The non-uniqueness of the fit is also found with two other simple models: a capillary-tube model with contact angle hysteresis and a spherical-pore model.

While this porous media model can fit the trend in the actual tank data, the fit must assume essentially equal sizes for pore throats and bodies, and this is unrealistic for typical porous media (Dullien 1992). In addition, to have sufficient bubble jumps in such pores requires very long bubbles. While there are no data for typical bubble length in porous media waste, long bubbles also seem unrealistic. Finally, the laboratory data for bubbles in sediment beds of sand show negligible hysteresis provided the pore space is filled with a Newtonian fluid (see Figures 6 and 7 at the lowest clay content). A more plausible mechanism for V-P hysteresis, which is bubbles displacing yield-stress fluids in a porous medium, is discussed in the following section.

Additional research concerned the yield stress and compressibility (the two properties of main interest) of a mixture of gas, liquid, and solids in the presence of surfactant. The yield stress of a mixture of foam and solids was investigated theoretically using 2D periodic model (Kam et al. 2002). The range of solid fractions considered was from about 39 to 68%. Figure 14 shows that the yield stress of a mixture increases with gas fraction at a given solid fraction and increases with solid fraction at a given gas fraction. At a fixed fraction of solid plus gas, the yield stress is relatively insensitive to gas or solid fraction alone. There exists a maximum liquid fraction above which the yield stress disappears. These trends agree with those reported for a mixture of foam and solids encountered in tunneling through soft sediments and proppant-laden fracturing fluids used in the petroleum industry. For sufficiently small solids and bubbles, capillarity significantly alters the compressibility of a dispersion of solids, liquid, and bubbles from that for the same volume of ideal gas and for a dispersion of bubbles of the same size without a solid present (Kam and Rossen 2002). There is a second-order phase transition at the point where bubbles touch each other between the solid particles.

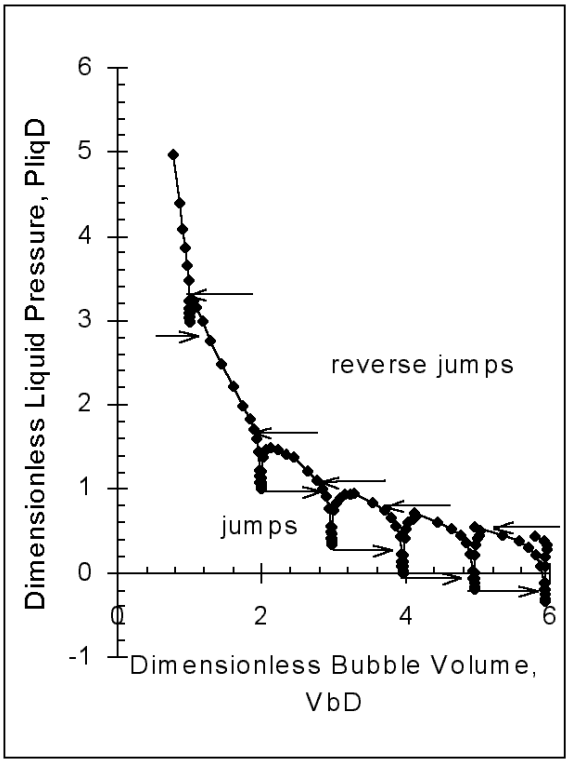

Figure 11. Response of a Volume of a Single Bubble Within a Porous Medium to Liquid Pressure Change at a Fixed Bubble Mass. If the pressure decreases, the bubble volume increases gradually until a jump to a larger volume occurs. From Kam et al. (2001a).

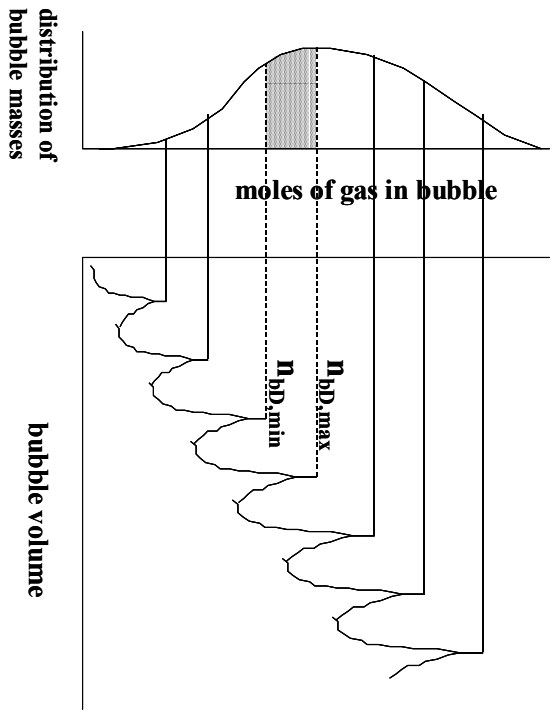

Figure 12. Schematic of Initial Distribution of a Population of Bubbles. A continuous distribution of bubble masses is analyzed in terms of the population between those (with $n_{bD,min}$ moles) that have just made one jump and those (with $n_{bD,max}$ moles) just about to make the next jump. The bottom of the figure is similar to Figure 11 (but with tracking bubble mass rather than pressure) turned on its side. From Kam and Rossen (2000).

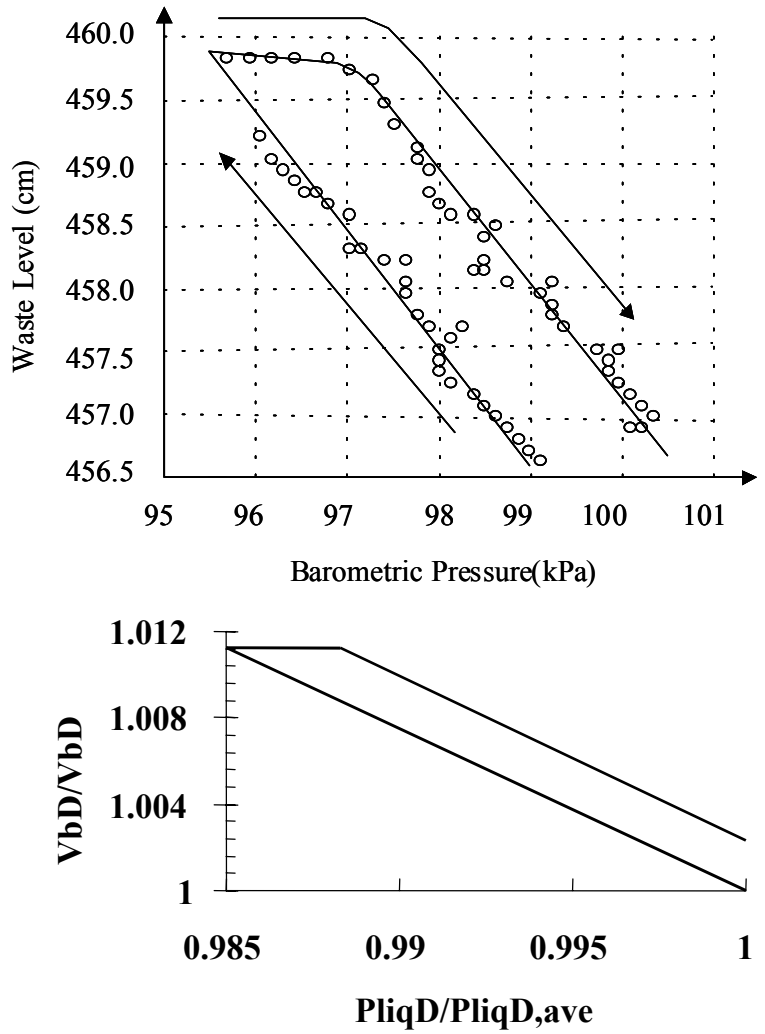

Figure 13. Fit of Models to Tank Data. Top: tank level during decrease and then increase in pressure (Whitney et al. 1996). Bottom: example of fit to trend of data; unfortunately, this fit is not unique, and compressibility of the gas, the goal of the study, cannot be determined uniquely from the fit. From Kam et al. (2001b).

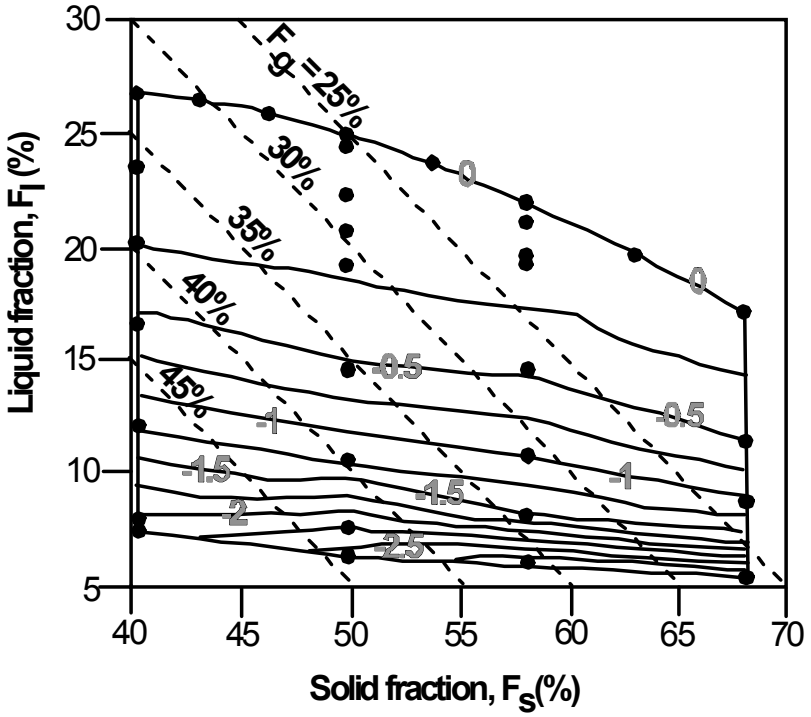

Figure 14. Predicted Dimensionless Yield Stress of Mixture of Bubbles and Sand as Function of Solids and Liquid Volume Fraction, from Kam et al. (2002). (Diagonal dashed lines indicate gas-volume fraction.) Contours with large gray numbers show values of maximum stress as bubbly sand is sheared; these values are of proportional to yield stress. Nearly horizontal contours means that yield stress depends on the volume fraction of the liquid but not separately on volume fractions of solids and gas.

2.2.4 Porous Media with Yield-Stress Fluids

Bubbles in rigid porous media filled with yield-stress fluids were studied to develop a model to explain the effective compressibility of bubbles in this unique waste microstucture. This section is devoted to the description of a model that was developed to investigate the effects of yield stress fluids and the mass transfer between liquid and gas phases on the pressure-volume lab experiments. This model does not account for the dynamics of fluid flow.

Figure 15 shows the simple model of a single bubble inside a capillary of radium R used to represent bubbles trapped in a porous sediment layer. One end of the tube is connected to a piston that increases or reduces pressure on the liquid phase to simulate external pressure in the lab experiment or barometric pressure in the Hanford waste tanks, while the gas phase is trapped in the other end of the tube. The distance between the piston and gas/liquid interface through the liquid phase is L. Even though, in reality, pores within the slurry of Hanford waste tanks have different radii and the gas/liquid interface is curved, we neglect these effects for simplicity and focus on mass transfer and yield stress.

For a yield stress fluid in a capillary tube, a minimum pressure difference of $\tau_o 2L/R$ is needed to displace the fluid slug (Bird et al. 1960). For small-diameter pores where individual bubbles may be

separated by many pores, it is reasonable for the ratio of L/R to be very large. It is this scaling that offers an explanation for how very weak yield-stress fluids can cause V-P hysteresis in porous media.

We define pressures P_g, P_{int}, and P_{ext} at three different locations along the capillary tube as pressure within gas phase, liquid pressure near the gas/liquid interface, and liquid pressure at the face of piston. With a flat gas/liquid interface, $P_g = P_{int}$. If $P_{int} = P_{ext}$ at the initial, equilibrium state, then the three pressures are the same initially ($P_g=P_{int}=P_{ext}$).

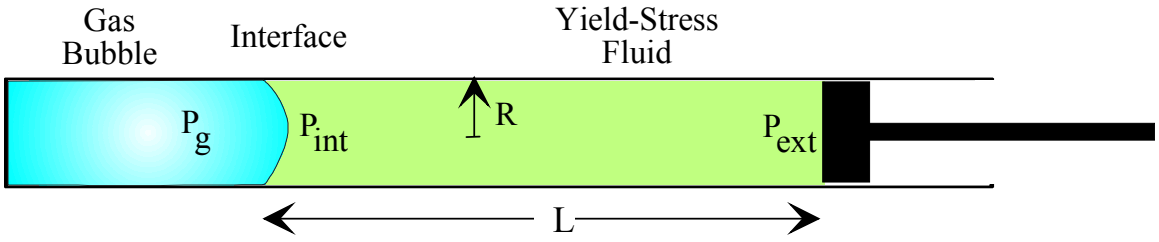

Figure 15. Model of Bubble Displacing a Yield-Stress Fluid in a Capillary Tube

Sinusoidal change in the external pressure in the lab experiment can be expressed as

$$P_{ext} = (P_{liq}^{o} - \frac{\Delta P}{2}) + (\frac{\Delta P}{2})\cos(\frac{2\pi t}{t^{o}}) \tag{15}$$

where P_{liq}^{o} is liquid pressure at the initial equilibrium state before moving the piston, ΔP is the maximum external pressure change, i.e., the amplitude of the cycle, and t^{o} is the period of each pressure-change cycle.

We consider, first, mass transfer alone. For simplicity, we assume that only one component "A" is volatile. Henry's law defines the equilibrium state at near gas/liquid interface:

$$P_g = H_A x_{A,int} \tag{16}$$

where H_A is Henry's constant for component A, and $x_{A,int}$ is the mole fraction of component A in the liquid phase near the gas/liquid interface. In the absence of capillary effects and yield stress and with the assumption of instantaneous diffusion across the gas/liquid interface, the transport of component A from bulk liquid phase to the gas/liquid interface (therefore, into gas phase) is governed by concentration difference; i.e.,

$$\frac{dn_g}{dt} = k_1(x_{A,\text{int}} - x_{A,bulk}) = k_1(\frac{P_g}{H_A} - x_{A,bulk}) = k_1(\frac{P_{\text{int}}}{H_A} - x_{A,bulk}) \tag{17}$$

where n_g is mole of component A in the gas phase, $x_{A,bulk}$ is mole fraction of component A in the bulk liquid phase, and k_1 is a proportionality constant, accounting for the diffusion rate.

The mass of component A leaving (or, entering) the liquid phase equals the mass gained (or, lost) in the gas phase. Therefore,

$$\frac{1}{k_2}\frac{dx_{A,bulk}}{dt} = \frac{dn_g}{dt} \tag{18}$$

where k_2 is a proportionality constant, accounting for the volume of a liquid reservoir.

Differentiating Eq 17 with respect to t and inserting $dx_{A,bulk}/dt$ from Eq 18 leads to the following second-order ordinary differential equation for mass transfer of volatile component A in a capillary tube:

$$\frac{d^2 n_g}{dt^2} + k_1 k_2 \frac{dn_g}{dt} = \frac{k_1}{H_A}\frac{dP_{\text{int}}}{dt} \tag{19}$$

Now consider a yield stress in the liquid phase. Suppose the liquid between the gas/liquid interface and a piston has a yield stress of τ_o. With this yield stress, a change in external pressure (P_{ext}) does not immediately alter the liquid pressure near the gas/liquid interface (P_{int}) or gas pressure (P_g). Instead, there is a minimum pressure change required to cause the gas/liquid interface to move in or out. The minimum pressure change required to move this interface (P_{ys}) is determined by the yield stress of the liquid (τ_o), tube radius (R), and the distance between the gas/liquid interface and the piston (L):

$$P_{ys=}\frac{\tau_o 2L}{R} \tag{20}$$

Suppose both a yield stress and mass transfer are active. If the external pressure decreases, but less than P_{ys}, even though the gas pressure and liquid pressure near the gas/liquid interface stays constant, diffusion from the bulk-liquid phase into the gas bubble can occur because of the pressure gradient inside the liquid phase. This complexity cannot be fully explained with this simple model. To take this effect of pressure gradient in the liquid phase into account qualitatively, we introduce the concept of a representative liquid pressure (P_{int}^{re}) near the gas/liquid interface, which is defined as follows.

$$P_{\text{int}}^{re} = \omega P_{ext} + (1-\omega)P_{\text{int}}^{ys} \tag{21}$$

where P_{int}^{ys} represents liquid pressure at the gas/liquid interface in the yield-stress model, and ω is a weighting factor. If ω=1, the representative liquid pressure (P_{int}^{re}) equals external pressure, giving the case of mass transfer only with no effect of yield stress. If ω=0, the representative liquid pressure (P_{int}^{re}) equals the liquid pressure at the gas/liquid interface P_{int}^{ys} of the yield-stress model, but still mass transfer occurs by P_{int}^{ys} (Note that ω=0 and k_1=0 gives the same results as the yield-stress model, neglecting the effect of mass transfer).

From Eq 19 and Eq 21, the governing equation with yield stress as well as mass transfer is as follows.

$$\frac{d^2 n_{gD}}{dt_D^2} + k_{1D} k_{2D} \frac{dn_{gD}}{dt_D} = -\frac{k_{1D}}{H_{AD}} \frac{dP_{\text{int}D}^{re}}{dt_D} \tag{22}$$

where dimensionless variables are identified by the subscript "D," and parameters are defined as follows: n_g is divided by n_g^o (moles of gas at the initial state); t by t^o (each cycle in external pressure change); k_1 by (n_g^o/t^o); all pressures (P_g , P_{int}, P_{ext}, P_{ys}, P_{int}^{ys}, P_{int}^{re}, and ΔP) and H_{AD} by P_{liq}^o; and gas volume (V_g) by V_g^o (gas volume at initial state corresponding to P_{liq}^o), while k_2 is multiplied by n_g^o. Once the moles of gas (n_{gD}) are determined as function of time, the gas volume (V_g) can be calculated by the ideal gas law with a given gas pressure (P_g).

An interesting feature of this model is that the yield-stress parameter, P_{ysD}, depends on both the yield stress and the ratio R/L, as shown by Equation 20. In porous media, a distribution of R/L is typical, rather than a single value, and a more realistic prediction for actual behavior would be a composite of many different pores. Accordingly, model predictions will also include results created by averaging the results from a number of yield-stress parameter values to create a composite result representing a distribution of R/L values.

Figure 16 shows model predictions for a range of dimensionless yield-stress values when the effect of mass transfer is negligible. Results are shown for both a single value of R/L and a simple distribution of R/L that is a composite result of three equally weighted R/L values. For these calculations, the parameter values for $k_{1D}*k_{2D}$ and k_{1D}/H_{AD} were set arbitrarily small to minimize the role of mass transfer. Because the ratio R/L is not readily determined independently, a range of the yield-stress parameter was used that seemed reasonable for the experimental conditions (P_{ysD} was set to 0.0012, 0.006, and 0.012). For both of the results in Figure 16, increasing the yield stress gives larger V-P hysteresis with the loop becoming wider with increasing yield stress. With a single value for R/L, the results are essentially a parallelogram with four sharp corners. The shallow-sloped top and bottom reflect the yield stress of the fluid resisting bubble expansion and compression (negligible volume change with pressure), and the sides of the parallelogram represent ideal gas behavior after the yield stress is exceeded. For the results with a distribution of three R/L values, the shape of the V-P hysteresis changes to have two of the four corners become curved. The curved corners reflect the different pores reaching the onset of yielding at different pressure changes. The other two corners remain sharp in the absence of mass transfer where the pressure switches from decreasing to increasing, or the reverse. The results for both a single value of R/L and a distribution of R/L agree with the general trend in the data presented in Section 2.1, and we used reasonable values for the parameters. Further comparison with data is discussed below.

Figure 17 shows how mass transfer shifts the shape of the V-P hysteresis loops. For this calculation, the parameters values were $k_{1D}*k_{2D} = 1$, $k_{1D}/H_{AD} = 0.6$, and ω=0.5. These parameter values represent the conditions in the experiments discussed in Section 2.1. The results show that mass transfer causes the corners in the V-P loops to become more round, even the two corners where the pressure switches the direction of change. An additional result is that with mass transfer being active, the bubble volume shows the distinctive overshoot when the pressure changes direction.

Figure 18 shows a comparison between the experimental results and the model that assumes a simple distribution of R/L for range of yield stress. This comparison illustrates that the model captures important features in the pressure-volume experiment: the slope of the V-P hysteresis loop deviates more and more from the ideal-gas behavior with increasing yield-stress, or bentonite concentration, and the loop becomes wider and then more horizontal with a monotonic increase in bentonite concentration.

In this initial theoretical approach, a simple model for the displacement of the yield-stress fluid was used rather than the more complicated approach of including residual stresses that we employed when analyzing spherical bubbles in infinite media. In spherical geometry, including residual stresses gave an order-of-magnitude difference in results in comparison to neglecting the residual stresses. The literature does not address how residual stresses might affect bubble expansion and compression in porous media and this remains a problem for future study.

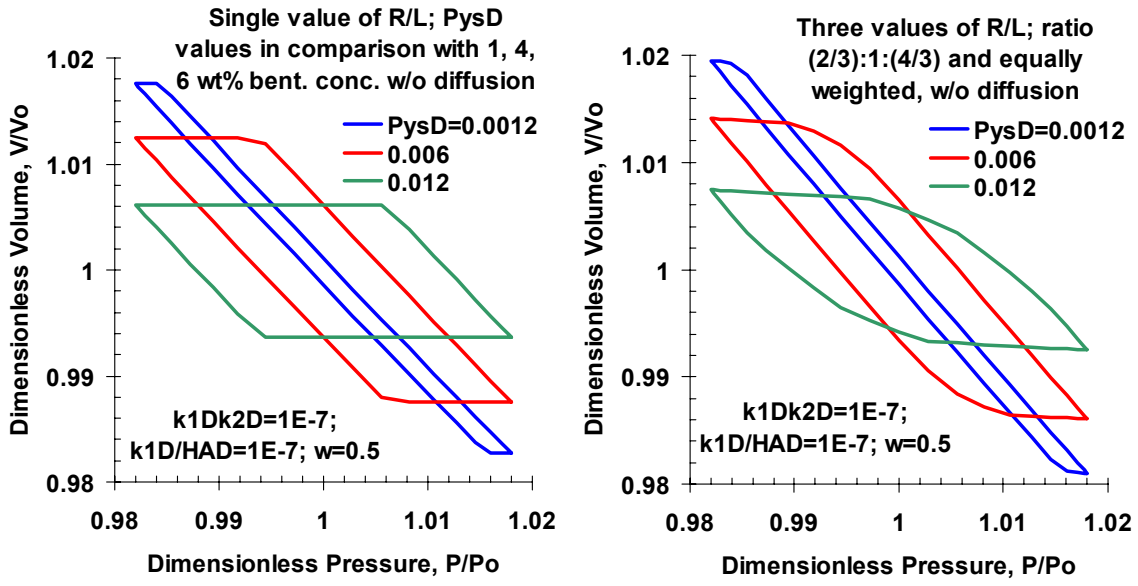

Figure 16. Effect of Yield Stress on P-V Hysteresis for a Single Value of R/L and a Simple Distribution of R/L with Mass Transfer being Negligible.

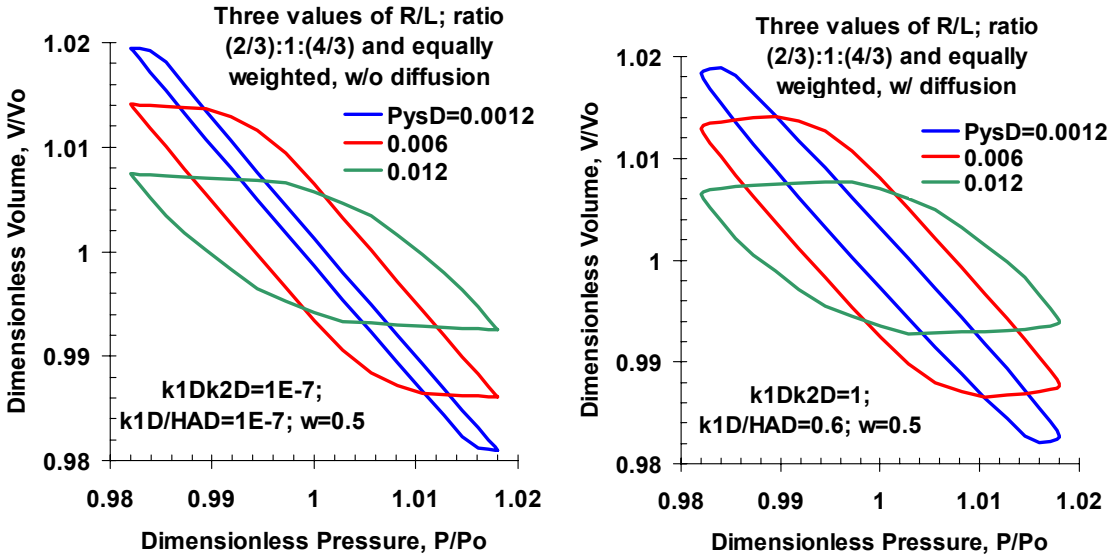

Figure 17. Comparison of Model Results with and Without Mass Transfer on V-P Hysteresis

3.0 Relevance, Impact, and Technology Transfer

For application to Hanford tanks, the most significant conclusion is that a new waste microstructure and bubble configuration must be postulated to explain the observed V-P hysteresis. Previous work had postulated either bubbles held in a continuum waste that behaved as a soft solid or bubbles trapped within the pore spaces of settled beds of salt crystals. While V-P hysteresis with both of these microstructures is predicted theoretically and observed experimentally, the parameter ranges with significant hysteresis do not match well with typical Hanford waste properties. Our studies, however, also discovered a new microstructure directly linked with the V-P hysteresis. The only reasonable microstructure to account for hysteresis is when the bubbles are trapped in the pore spaces of a settled bed of salt crystals, and the pore space itself is filled with a soft solid. This is a fundamentally new microscopic waste and bubble configuration.

This waste microstructure will impact future Hanford operations, such as salt-well pumping and salt-dissolution retrieval. For both of these waste operations, an underlying assumption is that liquid will drain from or percolate through the pore spaces of the beds of salt crystals. If the proposed microstructure exits in single-shell tanks with V-P hysteresis, these tanks have yield-stress fluids filling the pore spaces and drainage and percolation will be slowed. Waste operations will need to plan for added time in conducting operations in these waste tanks.

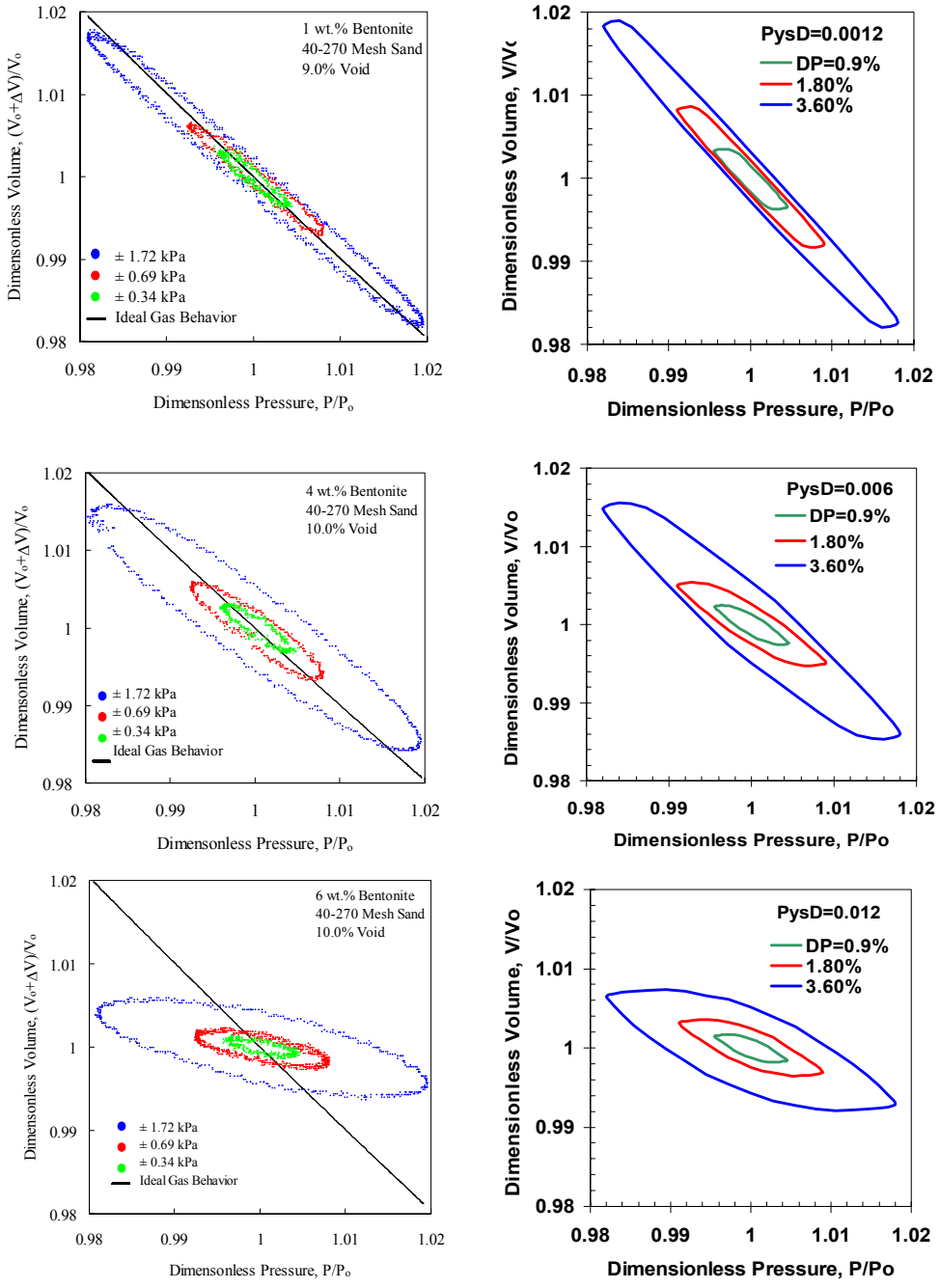

Figure 18. Comparison Between Model and Experimental Results for the Effect of Increasing Yield Stress on P-V Hysteresis for Bubbles in Porous Media

The fundamental understanding developed in this project continues to be relevant to a variety of waste-management issues. As an example, Terrones and Gauglitz are funded by the Hanford K-basin project to investigate the mechanics of bubbles in spent fuel sludges that will be retrieved from the Hanford K-basins. Both solid-mechanics and fluid-mechanics approaches are being used to address bubble behavior in 1.5-m-diameter vessels for inclusion in a formal safety analysis of long-term sludge storage. As an additional example, Rossen of the University of Texas at Austin participated in an expert panel on enhancing salt-well pumping performance that was organized by the Tanks Focus Area and held at Hanford in FY2001.

4.0 Project Productivity

The project achieved significant progress on each of the original objectives, though progress was delayed compared to the original schedule. The surprising absence of V-P hysteresis in the initial simulants planned for the experimental studies slowed the project schedule. Only when the new microstructure of a yield-stress fluid embedded in a porous media was discovered to be significant did the project achieve completion. The preliminary experiments showing this dramatic V-P hysteresis in porous media embedded with a yield-stress fluid occurred toward the end of the scheduled project, and the majority of the experiments and modeling for this novel microstructure to confirm the results were completed in the year following the scheduled completion of the study.

5.0 Personnel Supported

Dr. Phillip A. Gauglitz, Principal Investigator, Pacific Northwest National Laboratory

Dr. Morton M. Denn, Co-PI, Professor of Chemical Engineering, University of California, Berkeley

Dr. Susan J. Muller, Co-PI, Professor of Chemical Engineering, University of California, Berkeley

Dr. William Rossen, Co-PI, Professor of Petroleum and Geosystems Engineering, University of Texas at Austin.

Dr. Guillermo Terrones, Co-Principal Investigator, Pacific Northwest National Laboratory

Benjamin T. Liu, Graduate student research assistant, Department of Chemical Engineering, University of California, Berkeley

Dr. Seung I. Kam, Post Doctoral Research Associate, Department of Petroleum and Geosystems Engineering, University of Texas at Austin

Dr. Christopher L. Aardahl, collaborator, Pacific Northwest National Laboratory

Donny P. Mendoza, collaborator, Pacific Northwest National Laboratory

Travis B. Adamson, PNNL student intern, currently at Brigham Young University

Christopher M Kuffel, PNNL student intern, currently at Washington State University

Laurie Bachrach, PNNL student intern while in the Chemical Engineering Department, University of Washington.

6.0 Publications

Denn, M. M., and G. Marrucci. 1999. "Squeeze flow between infinite plates," *J. Non-Newtonian Fluid Mech.*, 87:175-178.

Gauglitz, P. A., S. I. Kam, and W. R. Rossen. "Bubble Expansion and Compression in a Porous Medium Filled with a Yield-Stress Fluid," in preparation, to be submitted to *J. Colloid and Inter. Sci.*

Gauglitz, P.A., G. Terrones, D. P. Mendoza, and C. L. Aardahl. 2000. "Behavior of Flammable Gas Bubbles in Hanford High-level Waste." In: *Proceedings of Waste Management 2000*, Tucson, Arizona, February 27 to March 2.

Kam, S. I. 1998. "Interactions between bubbles and solids: Three applications." Department of Petroleum and Geosystems Engineering, The University of Texas at Austin.

Kam, S. I., and W. R. Rossen, 2002. "The Compressibility of Foamy Sands," *Colloids and Surfaces A: Physicochemical and Engineering Aspects*, accepted and will appear.

Kam, S. I., P. A. Gauglitz, and W. R. Rossen, 2002. "The Yield Stress of Foamy Sands," *Colloids and Surfaces A: Physicochemical and Engineering Aspects*, accepted and will appear.

Kam, S. I., P. A. Gauglitz, and W. R. Rossen. 2001. "Effective Compressibility of a Bubbly Slurry: I. Theory of Behavior of Bubbles Trapped in Porous Media." *J. Colloid Interface Sci.*, 241(1), pp. 248-259.

Kam, S. I., P. A. Gauglitz, and W. R. Rossen. 2001. "Effective Compressibility of a Bubbly Slurry: II. Fitting Numerical Results to Field Data and Implications." *J. Colloid Interface Sci.*, 241(1), pp. 260-268.

Kam, S. I., and W. R. Rossen. 2000. "Diffusive Growth and Compressibility of Bubbles in Porous Media." In: *Proceeding at EuroConference on Foams, Emulsions and Applications,* Delft, The Netherlands, June 5–8, pp. 359-366.

Liu, B., S. J. Muller, and M. M. Denn. "Convergence of a regularization method for flow of a Bingham material about a rigid sphere," *J. Non-Newtonian Fluid Mech.*, submitted.

Terrones, G., and P. A. Gauglitz. "Deformation of a Spherical Bubble in Soft Solid Media Under External Pressure," in preparation, to be submitted to *Quarterly Journal of Mechanics and Applied Mathematics*.

7.0 Interactions

Gauglitz PA, G Terrones, DP Mendoza, MM Denn, SJ Muller, and WR Rossen. 1998. "Mechanics of bubbles in sludges and slurries: Initial progress." Hanford Technical Exchange, Richland, Washington, June.

Gauglitz, P. A. 2001. "Mechanisms of Gas Bubble Retention and Release: Laboratory Studies." In: *PNNL Hydrogen Conference*, invited presentation to BNFL and WGI, Warrington, UK, October.

Gauglitz, P. A., and J. H. Konynenbelt. 1997. "Mechanics of Bubbles in Sludges and Slurries: Preliminary Experiments." In: *AIChE Annual Meeting*, Los Angeles, California, November 16–21.

Gauglitz, P. A., G. Terrones, C. L. Aardahl, D. P. Mendoza, and L. A. Mahoney. 1999. "Mechanics of Bubbles in Sludges and Slurries: Experimental Studies and Solid Mechanics Modeling Results." In: *Engineering Foundation Conference on Rheology in the Minerals Industry II*, Oahu, Hawaii, March 14–19.

Gauglitz, P. A., G. Terrones, D. P. Mendoza, and C. L. Aardahl. 2000. "Behavior of Flammable Gas Bubbles in Hanford High-level Waste." In: *Waste Management 2000*, Tucson, Arizona, February 27 to March 2.

Gauglitz, P. A., G. Terrones, D. P. Mendoza, and C. L. Aardahl. 1999. "Elastic-Plastic Deformation of a Soft Solid by an Expanding Bubble." In: *The Society of Rheology: 71st Annual Meeting*, Madison, Wisconsin, October 17–21.

Gauglitz, P. A., G. Terrones, D. P. Mendoza, C. L. Aardahl, M. M. Denn, S. J. Muller, and W. R. Rossen. 1999. "Mechanics of bubbles in sludges and slurries." Presented to Hanford Site Technology Coordinating Group - Tank Subgroup, Richland, Washington.

Gauglitz, P. A., S. D. Rassat, and P. R. Bredt. 1998. "Mechanisms of Gas-Bubble Retention and Growth in Radioactive and Simulated Wastes," University of Washington, Chemical Engineering Department Colloquium, Seattle, Washington, February 23.

Gauglitz, P. A., S. D. Rassat, P. R. Bredt, and J. T. Aikin. 1998. "The Role of Waste Properties on Bubble Behavior and Estimates of Waste Strength from Horizontal Extrusions," University of California at Berkeley, Chemical Engineering Department, Polymer Group Seminar, March 17.

Kam, S. I., and W. R. Rossen. 1998. "Effective Compressibility of Gas Trapped in Porous Media." In: *Gordon Research Conference (Modeling of Flow in Permeable Media)*, Andover, New Hampshire, August 2-7.

Kam, S. I., and W. R. Rossen. 2000. "Diffusive Growth and Compressibility of Bubbles in Porous Media." In: *Proceeding at EuroConference on Foams, Emulsions and Applications*, Delft, The Netherlands, June 5–8.

Liu, B. T., S. J. Muller, and M. M. Denn. 2001. "Convergence of a regularization method for flow of a Bingham material about a rigid sphere," HSR 2001. In: *3rd International Meeting of the Hellenic Society of Rheology*, Patras, Greece, June.

Liu, B. T., S. J. Muller, and M. M. Denn. 2001. "Mechanics of two rigid spheres falling co-linearly in a Bingham material." In: *73rd Annual Meeting of the Society of Rheology*, Bethesda, Maryland, October.

8.0 Transitions

Within the Environmental Management programs of the DOE, many situations are continuing where bubbles of flammable gases are retained in beds of settled solids, and the basic studies conducted here have application. In addition to bubbles in underground HLW storage tanks, which is the focus of this study, bubble retention is a key issue for Hanford spent fuel sludge stored in canisters, and bubble retention occurs in process tanks and ion exchange beds in HLW pretreatment facilities. The fundamental understanding created in this project is being applied to these situations either through discussions with technical colleagues or through the direct involvement of the project staff.

One of the interesting findings of this project is the important waste microstructure of a yield-stress fluid within the pore space of a settled bed of larger particles. This microstructure and its unique behavior will impact future waste operations, such as salt-dissolution retrieval, and researchers working on these problems have been briefed on our findings.

9.0 Patents

None.

10.0 Future Work

Based on the results of this study, continued investigations are needed in a number of areas. The problem of small displacements of a yield-stress fluid within a porous medium needs more analysis. Our initial approach to this problem used a simple model for the displacement of the yield-stress fluid, rather than the more complicated approach of including residual stresses that we used when analyzing spherical bubbles. In spherical geometry, including residual stresses gave an order-of-magnitude difference in results in comparison to a simpler approach. The literature does not explain exactly how residual stresses affect bubble expansion and compression in porous media.

Further studies are also needed to determine the universality of the numerical approach we developed for locating the yield surfaces in complex flows. The essential problems that need to be addressed are interacting spheres and bubbles and the role that bubble-bubble interactions may play in enhanced rise velocities.

11.0 Literature Cited

Chadwick, P. 1959. "The Quasi-Static Expansion of a Spherical Cavity in Metals and Ideal Soils," *Quart. J. Mech. Appl. Math*., **12**, pp. 52-71.

Chhabra, R. P. 1993. *Bubbles, Drops, and Particles in Non-Newtonian Fluids*, CRC Press, Boca Raton, FL.

Dullien, F. A. L. 1992. *Porous Media: Fluid Transport and Pore Structure*, Academic Press, San Diego, CA.

Gauglitz, P. A., S. D. Rassat, P. R. Bredt, J. H. Konynenbelt, S. M. Tingey, and D. P. Mendoza. 1996. *Mechanisms of Gas Bubble Retention and Release: Results for Hanford Waste Tanks 241-S-102 and 241-SY-103 and Single-Shell Tank Simulants*. PNNL-11298, Pacific Northwest National Laboratory, Richland, Washington.

Hopkins, H.G. 1960. "Dynamic Expansion of Spherical Cavities in Metals," in Progress in Solid Mechanics, Snedon, I.N., and Hill, R. (eds.), North-Holland, Amsterdam, **1**, pp. 85- 164.

Kam, S. I., and W. R. Rossen. 2002. "The Compressibility of Foamy Sands," accepted and will appear in *Colloids and Surfaces A: Physicochemical and Engineering Aspects*.

Kam, S. I., and W. R. Rossen. 2000. "Diffusive Growth and Compressibility of Bubbles in Porous Media." In: *Proceeding at EuroConference on Foams, Emulsions and Applications,* Delft, The Netherlands, June 5–8.

Kam, S. I., P. A. Gauglitz, and W. R. Rossen. 2001a. "Effective Compressibility of a Bubbly Slurry: I. Theory of Behavior of Bubbles Trapped in Porous Media," *J. Colloid Interface Sci.*, 241(1), pp. 248-259.

Kam, S. I., P. A. Gauglitz, and W. R. Rossen. 2001b. "Effective Compressibility of a Bubbly Slurry: II. Fitting Numerical Results to Field Data and Implications," *J. Colloid Interface Sci.,* 241(1), pp. 260-268.

Kam, S. I., P. A. Gauglitz, and W. R. Rossen. 2002. "The Yield Stress of Foamy Sands," accepted and will appear in *Colloids and Surfaces A: Physicochemical and Engineering Aspects*.

Lubliner, J. 1990. *Plasticity Theory*, Macmillan Publishing Company, New York.

Powell, M. R., C. M. Gates, C. R. Hymas, M. A. Sprecher, and N. J. Morter. 1995. *Fiscal Year 1994 1/25-Scale Sludge Mobilization Testing*. PNNL-10582, Pacific Northwest National Laboratory, Richland, Washington.

Terrones, G., and P. A. Gauglitz. "Deformation of a Spherical Bubble in Soft Solid Media Under External Pressure," in preparation, to be submitted to *Quarterly Journal of Mechanics and Applied Mathematics*.

Whitney, P. D., P. A. Meyer, N. E. Wilkins, N. E. Miller, F. Gao, and A. G. Wood. 1996. *Flammable Gas Data Evaluation Progress Report*, PNNL-11373, Pacific Northwest National Laboratory, Richland, Washington.

Distribution

No. of Copies

OFFSITE

1 M. M. Denn
The Levich Institute
City College of CUNY
1-M Steinman Hall
140th Street at Convent Avenue
New York, New York 10031

1 S. I. Kam
Petroleum and Geosystems Engineering Department
University of Texas at Austin
Austin, Texas 78712

1 S. J. Muller
Chemical Engineering Department
University of California at Berkeley
Berkeley, California 94720

1 W. R. Rossen
Petroleum and Geosystems Engineering Department
University of Texas at Austin
Austin, Texas 78712

No. of Copies

ONSITE

1 **DOE, Richland Operations Office**
C. A. Groendyke H6-60

9 **CHG**
B. B. Barton R2-11
R. E. Bauer R4-01
B. J. Cash R1-04
K. A. Gasper L4-07
K. M. Hodgson R1-14
N. W. Kirch R3-73
R. E. Raymond R2-50
D. A. Reynolds R2-11
D. J. Washenfelder R2-12

1 **Numatec**
A-M. F. Choho R2-58

1 **Fluor Hanford**
D. L. Herting T6-07

1 **Los Alamos National Laboratory**
M. T. Terry K9-91

21 **Pacific Northwest National Laboratory**

C. A. Aardahl K8-93
P. R. Bredt P7-25
J. W. Brothers K7-15
P. A. Gauglitz (10) K6-28
J. L. Huckaby K7-15
D.P. Mendoza K6-81
P. A. Meyer K7-15
C. W. Stewart K7-15
G. Terrones K7-15
P. D. Whitney K5-12
Technical Report Files (2)